ESDU 05022
Issued January 2006

Extrapolating wind-tunnel data to full-scale Reynolds number.
Part 1: Principles

Endorsed by
The Royal Aeronautical Society

ESDU DATA ITEMS

Data Items provide validated information in engineering design and analysis for use by, or under the supervision of, professionally qualified engineers. The data are founded on an evaluation of all the relevant information, both published and unpublished, and are invariably supported by original work of ESDU staff engineers or consultants. The whole process is subject to independent review for which crucial support is provided by industrial companies, government research laboratories, universities and others from around the world through the participation of some of their leading experts on ESDU Technical Committees. This process ensures that the results of much valuable work (theoretical, experimental and operational), which may not be widely available or in a readily usable form, can be communicated concisely and accurately to the engineering community.

We are constantly striving to develop new work and review data already issued. Any comments arising out of your use of our data, or any suggestions for new topics or information that might lead to improvements, will help us to provide a better service.

THE PREPARATION OF THIS DATA ITEM

The work on this particular Data Item was monitored and guided by the Transonics Committee. This Committee first met in 1960 and now has the following membership:

Chairman	
Mr G.R. Hargreaves	— BAE SYSTEMS, Woodford
Vice-Chairman	
Mr G.R. Richards	— BAE SYSTEMS, Farnborough
Members	
Mr C. Burke	— Aircraft Research Association
Mr K. Burton	— BAE SYSTEMS, Brough
Mr A. Dyke	— Airbus, Bristol
Mr M.C.P. Firmin	— Member Emeritus
Mr J.L. Fulker	— QinetiQ, Aerospace Division, Bedford
Mr M.D. Hodges	— Independent
Mr T. Pemberton	— BAE SYSTEMS, Warton
Dr D.R. Philpott	— University of Hertfordshire, Hatfield
Dr S. Prince	— The City University, London
Dr S. Shaw	— Cranfield University, Bedfordshire
Mr D.R. Stanniland	— Aircraft Research Association
Mr P.W.C. Wong	— Aircraft Research Association Limited, Bedford

The construction and subsequent development of the Data Item was undertaken by

Dr D.R. Philpott	— Senior Engineer

The persons with overall responsibility for the work in this subject area are Dr M.M. Freestone and Dr D.R. Philpott.

EXTRAPOLATING WIND-TUNNEL DATA TO FULL-SCALE REYNOLDS NUMBER. PART 1: PRINCIPLES

EXTRAPOLATING WIND-TUNNEL DATA TO FULL-SCALE REYNOLDS NUMBER. Part 1: Principles

1. INTRODUCTION

Prediction of the flow around a full-scale aircraft from wind-tunnel tests on a smaller scale model is subject to a number of difficulties. Some of these are caused by obvious differences between the two situations, such as the presence of constraining walls in the wind tunnel. Other difficulties are caused by a failure to achieve the equality in non-dimensional parameters, such as Mach number and Reynolds number, which is essential to ensure equivalence between the model and full-scale cases.

As Reynolds number is the only significant non-dimensional parameter to involve the scale of the model, the use of a model of reduced scale normally makes it difficult to achieve equality in Reynolds number while matching other non-dimensional parameters. In particular this means that there are likely to be discrepancies in the boundary-layer state between the full-scale and sub-scale test cases. The effects of this mismatch may be exacerbated by such factors as the geometric complexity of the configuration under investigation, the degree of supercritical flow present, the strength and location of any shock waves and the presence of separated flow. The problem is, therefore, likely to be particularly significant in the transonic flow regime.

In order to formulate the requirements for and interpret the ensuing results of a wind-tunnel test it is essential to have a proper understanding of the factors that influence boundary-layer behaviour, particularly with regard to transition and separation. Thus an awareness of possible discrepancies between the sub-scale and full-scale cases may be developed and, where possible, suitable corrections made to wind tunnel data.

A further difficulty in the assessment of Reynolds number effects is caused by the fact that they may be confused with other effects inherent in wind-tunnel testing. For example, the boundary-layer growth on the wind-tunnel walls causes an effective change in the working section area, which varies with the state of the wall boundary layer. This effect may then be misinterpreted as a genuine Reynolds-number effect. Similar problems may arise if, for example, the Reynolds number is controlled by varying the tunnel stagnation pressure. In this case the change in dynamic pressure may cause significant model deflections. A third example is the effect on the boundary-layer that may occur if the model is at a significantly different temperature from that of the freestream.

Interpretation of these "pseudo Reynolds number" effects requires a broad understanding of the wind tunnel testing process. For this reason some care is taken in this Data Item to examine the assumptions implicit in the establishment of the non-dimensional parameters, on which rests the concept of dynamic similarity. Next there is a broad classification of the discrepancies between wind tunnel and full scale, followed by a review of the mechanisms involved in boundary-layer transition and separation. Finally a detailed review of "pseudo Reynolds number" effects is given.

Although much of this Data Item is applicable to general conditions on aircraft configurations, the practical emphasis is on transonic flows around aircraft having lifting surfaces of moderate sweep ($\leq$35 deg) and aspect ratio ≥ 4.

2. NOTATION

A	wave amplitude
a	speed of sound
A_N	wave amplitude at neutral stability point (see Section 5.1.1)
$B_{1\ldots n}$	non-dimensional groups relating to body forces
b	span
C_p	pressure coefficient
C_L	lift coefficient
c	chord of aerofoil, or local wing chord
$\bar{c}$	wing mean chord
c_p	specific heat at constant pressure
c_v	specific heat at constant volume
d_e	excrescence width, normal to local flow direction
e	excrescence height
$\vec{f}$	body force vector
H	specific enthalpy
k	thermal conductivity
l	characteristic length
M	Mach number
M_{shock}	Mach number immediately upstream of shock wave on aerofoil
N	Tollmien-Schlichting wave amplification exponent (Equation (5.2))
p	pressure
p_{out}	pressure at outlet of supersonic nozzle (Sketch 3.1)
$\vec{q}$	velocity vector
R	gas constant
Re	Reynolds number, (= $U_\infty \bar{c}/\nu$ for wing, or = $U_\infty c/\nu$ for aerofoil)

Re_e	excrescence Reynolds number, (= $u_e e/\nu$)
Re_l	Reynolds number, (= $U_\infty l/\nu$)
Re_x	Reynolds number based on distance, x, from leading edge of flat plate, (= $U_\infty x/\nu$)
$Re_{s_{stag}}$	Reynolds number based on distance from stagnation point, (= $U_\infty s_{stag}/\nu$)
Re_{xe}	Reynolds number based on distance of excrescence from leading edge of flat plate and velocity at edge of boundary layer, (= $u_\delta x_e/\nu$)
$Re_{\delta e}$	Reynolds number based on height of excrescence and velocity at edge of boundary layer, (= $u_\delta e/\nu$)
Re_θ	Reynolds number based on momentum thickness, (= $U_\infty \theta/\nu$)
$Re_{\delta *}$	Reynolds number based on displacement thickness, (= $U_\infty \delta^*/\nu$)
$Re_{\delta T}$	flat plate transition Reynolds number, (= $u_\delta x_T/\nu$)
r_0	surface radius of curvature in streamwise direction
S_t	wind tunnel working section cross-sectional area
S_{ref}	reference area
s_{stag}	distance measured from stagnation point
T	temperature
T_u	freestream turbulence intensity, (= $\sqrt{u'^2}/U_\infty$)
T_δ	non-dimensional turbulence intensity, (= $\left(\overline{u'^2}+\overline{v'^2}+\overline{w'^2}\right)^{1/2}/(3u_\delta)$)
t	time variable
$\hat{t}$	non-dimensional time variable, (= tU_∞/l)
U_∞	freestream velocity
u, v, w	velocity components in x, y and z directions respectively
u_e	local velocity at excrescence height, within boundary layer
x, y, z	cartesian coordinates
x_e	distance from leading edge of flat plate to location of excrescence

x_n	distance from leading edge at which Tollmien-Schlichting instability occurs
x_{pg}	distance from beginning of pressure gradient to separation point
x_{shock}	distance from aerofoil leading edge to origin of sidewall shock wave
x_T	distance from leading edge of flat plate to full transition (fully turbulent flow)
$\hat{x}$	non-dimensional coordinate, $(= x/l)$
$\hat{y}$	non-dimensional coordinate, $(= y/l)$
$\hat{z}$	non-dimensional coordinate, $(= z/l)$
ΔM	Mach number error (Equation (8.1))
Y	strain related dissipation term in energy equation (Equation (3.5))
α	incidence, or non-dimensional wave number, $(\alpha = 2\pi\delta^*/\lambda)$
β	angle between shock wave and upstream velocity vector
γ	ratio of specific heats, $\left(= \frac{c_p}{c_v}\right)$
δ	boundary layer thickness
δ^*	boundary layer displacement thickness
θ	boundary layer momentum thickness
θ_s	change in flow direction through shock wave
Λ	wing leading edge sweep angle (see Sketch 5.12)
λ	wavelength of Tollmien-Schlichting wave
μ	shear coefficient of viscosity
μ_b	bulk coefficient of viscosity
ν	kinematic viscosity, $\left(= \frac{\mu}{\rho}\right)$
ρ	density
σ	relative humidity
τ_w	shear stress at wall

Other Subscripts

attachment line	denotes value relating to attachment line at wing leading edge
N	denotes Reynolds number for neutral stability
T	denotes value at which transition to fully turbulent flow occurs
crit	denotes critical value
*crit*1	denotes value at which a vortex street is first generated by an excrescence
*crit*2	denotes value at which a fully turbulent wake is generated by an excrescence
eq	denotes wall equilibrium value
plen	denotes value in plenum chamber
stag	denotes stagnation value
s_{stag}	denotes distance from stagnation point
w	denotes value at wall
δ	denotes value at edge of boundary layer
∞	denotes freestream value
1	denotes value upstream of shock wave
2	denotes value downstream of shock wave
mean N to T	denotes average value between neutral stability and onset of transition

Superscripts

'	denotes non-steady velocity or component thereof (*e.g.* $u' = (u - \bar{u})$)
-	denotes time averaged quantity (*e.g.* $\bar{u} = \frac{1}{2\Delta t}\int_{t-\Delta t}^{t+\Delta t} u.\mathrm{d}t$, where Δt is large compared with the period of the lowest frequency under consideration)

3. DYNAMIC SIMILARITY IN INCOMPRESSIBLE AND COMPRESSIBLE FLOWS

3.1 Dimensional Analysis

Standard texts, *e.g.*[1,2], introduce the concepts of dimensional analysis and dynamic similarity by appealing to the fact that any expression relating physical quantities must be dimensionally consistent. For example, expressions describing the behaviour of variables in a system governed by Newtonian physics must be homogeneous in three basic dimensions, such as (mass, length and time) or (force, length and time) *etc*. The parameters relevant to the problem are usually chosen by an intuitive appreciation of the physical basis of the problem.

To illustrate this, consider the classic problem of steady flow past a body immersed in an incompressible freestream. The variable under examination is the pressure $p(x,y,z)$. The relevant parameters may be chosen as the freestream speed, U_∞, density ρ, viscosity μ and a characteristic dimension, l. Dimensional analysis, using the methods of [1,2], gives:

$$\frac{p(\hat{x},\hat{y},\hat{z})}{\rho U_\infty^2} = \mathrm{f}\left(\frac{\rho U_\infty l}{\mu}\right) = \mathrm{f}\,(Re_l). \tag{3.1}$$

This is usually written alternatively in terms of pressure coefficient:

$$C_p(\hat{x},\hat{y},\hat{z}) = \frac{p-p_\infty}{\frac{1}{2}\rho U_\infty^2} = \mathrm{f}\,(Re_l). \tag{3.2}$$

In this expression the pressure coefficient and the Reynolds number are both non-dimensional and the pressure coefficient variation is specified in terms of a coordinate system $(\hat{x},\hat{y},\hat{z})$ scaled with respect to the characteristic length, l. There is a direct equivalence between two flows around geometrically similar bodies (subject to the stated restrictions) which have the same freestream direction and Reynolds number, even though the values of U_∞, l, ρ and μ may differ between these flows.

A preferable (to intuition) method of selecting the relevant parameters for inclusion in the dimensional analysis is by appeal to the governing equations. In fluid dynamics these are well known, although an analytic solution to a particular problem may not exist. A proper examination of these equations, and the assumptions implicit in their formulation, promotes a clearer understanding of the appropriate parameters to be included in the dimensional analysis and of the significance of the resulting dimensionless groups. This approach is adopted here. The complete governing equations are extremely complex. Care is taken to introduce them in a general form but details of derivation and the structure of particular terms are not presented, as these details are not essential for the purpose of this Data Item.

3.2 Examination of the Governing Equations

If air flows past an object which is large compared with the mean free path of the molecules of which the air is comprised, then the dynamics of the individual molecules may be ignored and the air treated as a continuous distribution of matter in space, or *continuum*. Since the mean free path in the Standard Atmosphere[3] is only 6.68×10^{-7} m even at an altitude of 18000 m, this assumption may reasonably be made for conventional aircraft. The motion of such a continuum is governed by partial differential equations expressing the conservation of mass and momentum. In the case of a Newtonian fluid (defined as having strain-independent coefficients of viscosity, μ, μ_b) these equations are[4]:

the Navier-Stokes equation:

$$\frac{\mathrm{d}\vec{q}}{\mathrm{d}t} = -\frac{1}{\rho}\nabla p + \frac{\mu}{\rho}\nabla^2\vec{q} + \frac{\left(\mu_b + \frac{1}{3}\mu\right)}{\rho}\nabla(\nabla.\vec{q}) + \vec{f} \quad , \tag{3.3}$$

(where the total derivative) $\frac{\mathrm{d}\vec{q}}{\mathrm{d}t} = \frac{\partial\vec{q}}{\partial t} + (\vec{q}.\nabla)\vec{q})$

and the continuity equation:

$$\frac{\partial\rho}{\partial t} + \nabla.(\rho\vec{q}) = 0\,. \tag{3.4}$$

The Navier-Stokes Equation (3.3) (sometimes referred to as the momentum equation) expresses the momentum changes due to body and boundary forces. The second and third terms on the right hand side of Equation (3.3) are the "viscosity" terms, caused by molecular diffusion, and are discussed further in Section 3.3.2.2. The continuity Equation (3.4) simply expresses the conservation of mass.

Expanding the vector form of the Navier-Stokes Equation (3.3) gives three momentum equations, corresponding to the three coordinate directions. Together with the continuity Equation (3.4) and appropriate boundary and initial conditions, these equations may be solved (although not, in general, analytically) for the three components of the velocity, $\vec{q}$, and the pressure, p, *provided that the flow is incompressible* (*i.e.* ρ is constant).

In the case of a compressible flow, other information is required, since ρ is no longer constant. The energy equation[4] is therefore introduced:

$$\frac{\mathrm{d}H}{\mathrm{d}t} = \frac{1}{\rho}\frac{\mathrm{d}p}{\mathrm{d}t} + \frac{1}{\rho}Y + \frac{1}{\rho}\nabla.(k\nabla T)\,. \tag{3.5}$$

This equation expresses the change of internal energy in the fluid caused by heat transfer and boundary stresses. The term, Y, is the viscous energy dissipation governed by the coefficients of viscosity μ and μ_b. The last term deals with the energy exchange due to thermal conductivity. The significance of μ_b is discussed further in Section 3.3.2.2.

For a perfect gas the specific enthalpy may be written:

$$H = c_p T\,. \tag{3.6}$$

The introduction of the temperature, T, both here and in the heat conduction term, requires the addition of the equation of state:

$$\frac{p}{\rho} = RT\,. \tag{3.7}$$

For a perfect gas, R is constant. If c_p is also constant, the gas is calorically perfect. These conditions are closely approximated by dry air at temperatures and pressures typical of the operating conditions for conventional aircraft.

Because of the introduction of relationships relating to thermodynamic processes in addition to Newton's laws, it appears that the list of basic dimensions should be extended to become mass, length, time and temperature. The introduction of these two equations also implies that the additional gas properties, R and c_p, should be included in the list of relevant parameters in the dimensional analysis.

However, since $R = (c_p - c_v) = c_p\left(\frac{\gamma-1}{\gamma}\right)$ and the speed of sound $a^2 = \gamma RT$:

$$H = \frac{a^2}{\gamma - 1}. \tag{3.8}$$

Also, if the thermal conductivity, k, is a constant, the last term in the energy equation (3.5) can be written as $\frac{1}{\rho}\nabla.(\nabla(kT))$ where

$$kT = \frac{ka^2}{\gamma R}. \tag{3.9}$$

Since these are the only two terms containing temperature in the governing equations, the speed of sound, a, can be used as a variable instead of T. This reduces the list of fundamental dimensions back to the original mass, length, time, as a can be described solely in terms of length and time. The relevant fluid property relating to heat transfer then becomes, $\frac{k}{\gamma R}$ and that relating to H is γ.

For the flow of a uniform air stream around a given shape, Equations (3.3), (3.4), (3.5), (3.7), (3.8) and (3.9) determine the distribution of the values of the variables $\vec{q}$, p, ρ and a over the flow field. To define the problem fully, further information is required. First it is necessary to specify boundary conditions at any solid surface. These are the zero velocity ("no slip") condition, and conditions sufficient to determine heat transfer rates at the surface. Unless there is zero heat transfer at the surface (adiabatic surface conditions) this requirement makes it necessary to introduce the surface temperature, T_w. Next, the freestream conditions U_∞, ρ_∞, a_∞ are required. T_∞ must also be specified if the solid boundaries are not adiabatic. In this case the temperature must now be introduced as a fourth dimension, extending the list of fundamental dimensions to *mass*, *length*, *time* and *temperature*. However, this is only necessary if heat transfer at the walls is of significance and gives rise to the addition of a single additional group, a temperature ratio, in the dimensional analysis (Equation (3.10)). Finally the fluid properties μ, μ_b, $\frac{k}{\gamma R}$, γ and the characteristic length, l must be specified. In the case of an unsteady flow, appropriate initial conditions may also be required. Using the parameters in the dimensional analysis gives, for the pressure coefficient in compressible flow*:

$$C_p(\hat{x}, \hat{y}, \hat{z}, \hat{t}) = \mathrm{f}\left(Re_l,\ M_\infty,\ \gamma,\ \frac{\mu_b}{\mu},\ \frac{(k/\gamma R)}{\mu},\ \frac{T_w}{T_\infty},\ B_1,\ B_2, \ldots\ldots\right)$$

* As this expression is generalised for unsteady flows, C_p depends on the non-dimensional time parameter $\hat{t} = (tU_\infty/l)$ in addition to the three space-coordinates $\hat{x}, \hat{y}, \hat{z}$. Thus $\hat{t}$ is included on the left hand side of this equation and in Equation (3.10). The groups B_n relate to the body forces, $\hat{f}$, and will depend on the nature of the body force, *e.g.* gravitational, electromagnetic *etc*. (See Section 3.3.1)

Since γ already appears on the right hand side of this equation and $R = c_p\left(\frac{\gamma-1}{\gamma}\right)$, the non-dimensional group $\frac{(k/\gamma R)}{\mu}$ may be replaced with the more familiar Prandtl number $\frac{\mu c_p}{k}$, so that:

$$C_p(\hat{x}, \hat{y}, \hat{z}, \hat{t}) = \mathrm{f}\left(Re_l, M_\infty, \gamma, \frac{\mu_b}{\mu}, \frac{\mu c_p}{k}, \frac{T_w}{T_\infty}, B_1, B_2, \ldots\ldots\right). \tag{3.10}$$

3.3 Simplifying the Governing Equations

Certain simplifying assumptions have already been made in the governing equations; for example the assumption that the fluid is a continuum and that the thermal conductivity, k, is constant, as are γ and R. It is also assumed that the coefficients of viscosity, μ and μ_b are constant, although it is known that μ typically depends on temperature (Section 3.3.2.2). In this section, terms in Equation (3.10) are examined with regard to their relevance to the flow fields encountered in typical aeronautical applications. This allows further simplifying assumptions to be made while identifying those respects in which the finally adopted model differs from the exact solution.

3.3.1 Body forces

Normally the only body forces of interest in the flow of air around a conventional aircraft are those due to gravity. Examination of orders of magnitude for the terms in Equation (3.5) indicates that the body force contribution is typically less than 0.05% of the $\mathrm{d}p/\mathrm{d}t$ term. The contribution of the body forces is similarly insignificant in the momentum equation (Equation (3.3)). In most practical cases the B_n terms in Equation (3.10) may be therefore ignored.

3.3.2 Molecular-diffusion effects

In air, the primary physical reason for the existence of thermal conductivity and viscosity is molecular diffusion between adjacent "layers" of fluid. Thermal conductivity is caused by the diffusion of molecules across a temperature gradient and viscous stresses by the diffusion of molecules within a shear layer or boundary layer.

3.3.2.1 Thermal conductivity

The thermal conductivity of air is 0.02534 W/mK at Standard sea level conditions[5]. The heat transfer term $\nabla.(k\nabla T)$ in Equation (3.5) depends on the second derivative of temperature, T, or, from Equation (3.9) the second derivative of a^2. Again, examination of the orders of magnitude for Equation (3.5) shows that, for transonic flow, the heat conduction terms are typically of the order of 0.001% of the $\mathrm{d}p/\mathrm{d}t$ term. This is because of the low values of both k and the second derivatives of temperature. The contribution of the thermal conductivity terms is therefore negligible except in cases where the temperature difference between a boundary, such as a solid wall, and the surrounding flow is significant, or where shock waves are present. In the latter case the second derivative of the temperature across the shock wave is very high. However, because the thickness of the shock wave is comparable to the mean free path of the molecules, the assumption of continuum flow is violated and the set of differential Equations, (3.3), (3.4) and (3.5) must be replaced by the oblique shock wave equations (Section 3.3.3) which relate flow parameters across a shock wave. Thus the thermal conductivity may be neglected in regions in which the differential equations are valid. An exception to this is where solid surfaces have a temperature significantly different from that of the local flow. This is referred to again in Section 4.2.1

3.3.2.2 Coefficients of viscosity, μ and μ_b

The coefficient of viscosity, μ, is associated with the shear stresses on a fluid element caused by molecular diffusion across the element boundary. These stresses arise when there is a velocity gradient normal to the direction of flow. For dry air, under Standard sea level conditions[5], the value of μ is 17.894×10^{-6} Ns/m^2.

The bulk coefficient of viscosity, μ_b, is associated with the normal stresses, additional to those due to the equilibrium pressure, which are produced by molecular diffusion across the fluid element boundary. These stresses arise because of the rate of dilation, and the mean of their principal components is equal[4] to $\frac{\mu_b}{\rho}\frac{d\rho}{dt}$. Because these stresses are only significant when very high rates of dilation are present, μ_b is very difficult to measure experimentally[4], but arguments based on the kinetic theory of gases indicate[4] that it is of similar magnitude to μ.

The coefficient of viscosity, μ, is temperature dependent and varies according to Sutherland's law[5]. Strictly interpreted, this would modify Equations (3.3) and (3.5) to include the derivative terms of μ and, similarly other properties, such as μ_b. However these derivative terms are of little significance and are usually ignored.

Because the coefficients of viscosity are very small, the viscous terms are only of significance in Equation (3.3) when the associated velocity derivatives are very high. Generally this condition only occurs for the second term on the right hand side of Equation (3.3) in boundary layers or shear layers. The third term is primarily concerned with volume dilation rates. This term is generally insignificant but becomes large across a shock wave. However, this region must be determined using the oblique shock wave equations (Section 3.3.3). Similar arguments to those given in Section 3.3.2.1 allow terms involving μ_b to be discounted in the energy Equation (3.5).

3.3.3 Oblique shock wave equations

Across a shock wave the governing differential equations must be replaced by the oblique shock wave equations. These equations express mass and energy continuity and momentum balance across the shock considered as a discontinuity and are a generalisation of the Rankine-Hugoniot equations[6]. Examination of the full oblique shock wave equations[6] shows that the ratios p_2/p_1, ρ_2/ρ_1, M_2/M_1 and a_2/a_1 together with the local inclination, β, of the shock wave to the upstream velocity vector, may all be written in the form $f(M_1,\gamma,\theta_s)$. The oblique shock wave equations thus provide a link between the values of p, ρ, M and a in the two regions of continuum on either side of the shock wave. The change in flow direction, θ_s, across the shock wave is defined by the change in the velocity vector from $\vec{q}_1$ to $\vec{q}_2$, whilst the variation of $\vec{q}$ within the continuous regions is defined by Equations (3.3) to (3.5).

To obtain a solution to the governing equations, the introduction of shock waves may be required in order to allow the boundary conditions to be satisfied. A simple example of this is the one-dimensional supersonic flow in a nozzle, where the position of the normal shock wave in the duct is determined by the requirement for the pressure at the duct exit to equal the value, p_{out}, imposed as a boundary condition on the exit plane (Sketch 3.1).

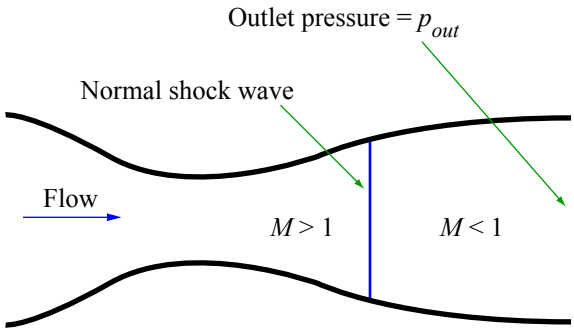

Sketch 3.1 Formation of Normal Shock Wave in a Supersonic Duct

Since the oblique shock wave equations do not introduce any new parameters, Equation (3.10) applies even when shock waves are present.

Although the flow mechanism within the shock wave results in a significant increase in entropy, neither viscosity nor heat transfer coefficients appear in the oblique shock wave equations. Thus the simplifications introduced in Sections 3.3.1 and 3.3.2 still apply.

3.4 Simplified Dimensional Analysis and Dynamic Similarity

The oblique shock wave equations are used to replace the governing differential equation across any shock wave. This means that there are no regions in which thermal conductivity, k, and the coefficient of viscosity, μ_b, are of importance. Further, it is established in Section 3.3.1 that the body forces, B_n, are insignificant. These parameters may now be omitted and Equation (3.10) reduces to:

$$C_p(\hat{x}, \hat{y}, \hat{z}, \hat{t}) = \mathrm{f}(Re_l, M_\infty, \gamma). \tag{3.11}$$

Thus, to obtain an equivalence between the flows around two geometrically similar objects, not only must the previously stated assumptions regarding the governing equations be valid but the Reynolds number, Re_l, the Mach number, M_∞, and ratio of specific heats, γ, must be identical in both cases. In addition the boundary and initial conditions must also be equivalent. If all these conditions are met, the two flows are said to be *dynamically similar*.

4. DISCREPANCIES BETWEEN WIND-TUNNEL AND FULL-SCALE RESULTS

Discrepancies between wind-tunnel and full-scale results may be caused by a failure to ensure dynamic similarity or by other factors such as instrumentation errors. In this Data Item, only problems caused by failure to achieve dynamic similarity are addressed.

From the analysis in Section 3 it is seen that failure to achieve dynamic similarity can have three basic causes:

violation of assumptions in governing equations,

failure to match boundary (or initial) conditions,

failure to match the non-dimensional parameters, Re_l, M_∞ or γ.

These are discussed further in Sections 4.1, 4.2 and 4.3.

4.1 Assumptions in Governing Equations

The assumptions in the governing equations are not limiting in tests up to supersonic speeds. An exception to this is the effect of humidity. Not only does humidity modify the value of the ratio of specific heats, γ, but latent heat may provide a significant additional term in the energy equation (Equation (3.5)) due to possible condensation and also subsequent evaporation. Other factors, such as energy release due to molecular dissociation, are not significant until hypersonic speeds (M_∞ greater than approximately 6) are reached. Humidity effects are discussed further in Section 8.3.3.

4.2 Matching Boundary and Initial Conditions

4.2.1 Boundry conditions

For a subsonic freestream it is not possible to match the boundary conditions between the "free-flight" case and a wind-tunnel test. In the "free-flight" case, the boundary conditions are applied at an infinite distance from the vehicle while, in the case of a wind-tunnel test, the best that can be done is to ensure uniform conditions at the entry to the working section with the tunnel empty. In all tunnel tests there is also an unsteady component in U_∞ due to turbulence in the tunnel circuit. Steps may be taken to minimise this but it cannot be eliminated. A further complication is that flow in the working section of a wind tunnel is bounded by solid walls, a constant pressure boundary (in an 'open-jet' wind tunnel) or, in the case of a transonic tunnel, perforated or slotted walls.

The above features are inherent in wind-tunnel testing. The other important part of the boundary representation is the model itself. Because of the small scales used in most wind tunnel tests, it is not possible to reproduce fine detail that may have a significant effect on the flow, particularly in the boundary layer. Generally, too, the model may deflect under aerodynamic load in a manner that is unrepresentative of the full-scale aircraft.

In Section 3.3.2.1 the significance of heat transfer from a solid surface is mentioned. This can be important, particularly in intermittent tunnels where there may be substantial differences between the temperatures of the air and the model surface.

4.2.2 Initial conditions

In the majority of cases, wind-tunnel tests are conducted with constant freestream conditions and, although a naturally unsteady flow (such as a wake oscillation) may result, specific matching of initial conditions is not required. In some cases, such as store release, time dependency is an essential element of a test. In this particular example, the initial conditions are self evident, although additional scaling parameters have to be introduced into Equation (3.10) in order to account for the dynamics of the store.

4.3 Matching Non-dimensional Parameters

4.3.1 Matching γ

According to kinetic theory[6], γ is dependent on the number of degrees of freedom of each molecule. According to these assumptions, for a gas comprising monatomic molecules, $\gamma = 1.67$, for diatomic molecules $\gamma = 1.40$ and for triatomic molecules $\gamma = 1.33$. Air is comprised mainly of diatomic molecules (O_2 and N_2) and consequently $\gamma \approx 1.40$. Close matching in γ is therefore obtained in tunnels using dry air or any other diatomic gas, such as nitrogen, which is frequently used as the working fluid in cryogenic wind tunnels.

4.3.2 Matching Re_l and M_∞

In any flow in which compressibility effects are important and shock waves are likely to be present, it is essential to match Mach number between tests at sub-scale and full scale. The difficulty in obtaining simultaneous Reynolds and Mach number matching in most conventional wind tunnels is well known. Where there is little or no control over the density or the coefficient of viscosity, the only way in which equality of Reynolds and Mach number may be maintained between the wind-tunnel test and full scale is to increase the freestream speed in inverse proportion to the model scale. This leads to an unacceptable mismatch in Mach number. Simultaneous Reynolds and Mach number matching may be achieved by the use of pressurised tunnels, which enable the density to be controlled, or cryogenic tunnels in which the air is cooled to allow a simultaneous reduction in viscosity and increase in density. The use of wind tunnels of this type confers an obvious advantage in the prediction of full-scale behaviour. However economic considerations often dictate that a significant proportion of a test program must be conducted in less expensive facilities, where a mismatch in Reynolds number between test and full scale must be accepted.

4.3.3 Dependence of the boundary layer on Reynolds number

In Section 3.3.2.2 it is seen that viscous stresses are significant only in boundary layers and shear layers where large second derivatives in velocity, normal to the local stream direction, are present. These conditions are met in the boundary layer close to a solid surface. Across this layer, there is a rapid increase in velocity from zero at the surface to the edge of the layer, where viscous stresses become negligible. It is known that the flow in the boundary layer may be laminar or turbulent and that it may also separate from the surface, forming a separation bubble or, if reattachment does not take place, a wake. The state of the flow within the boundary layer can thus have a very important bearing both on local flow near the surface and in the wider flow field. Both Reynolds number and external flow characteristics, such as freestream turbulence, influence transition from laminar to turbulent flow in the boundary layer and the separation location. The streamwise pressure gradients, external to the boundary layer, are also of critical importance and are particularly important at transonic speeds when shock waves occur. A number of different mechanisms may be involved in transition and separation, so that accounting for discrepancies between model tests and full scale may be difficult. A brief review of the transition and separation processes, partly based on the account of Young[7], is given in Sections 5 and 6 to help in the subsequent analysis of these discrepancies.

5. BOUNDARY-LAYER TRANSITION

Generally wind-tunnel tests are made at a Reynolds number considerably below the full-scale value and in an air stream with significant turbulence and acoustic noise. This is likely to lead to substantial differences in the boundary layer transition location between the sub-scale and full-scale cases, unless transition is fixed by artificial means. In a wind tunnel test at low Reynolds number, transition locations on a wing are, typically, significantly further downstream, in terms of non-dimensional distance, than is the case at full scale. It is also likely that the transition mechanisms differ between the two cases. Therefore, a correct interpretation of wind-tunnel results necessitates an understanding of the nature of these mechanisms and the factors that influence them.

The process of transition from laminar to turbulent flow within the boundary layer is caused by the growth of small disturbances, which extract energy from the surrounding fluid stream. The disturbances may originate from a number of sources and various factors may influence their damping or rate of amplification. In Sections 5.1 to 5.1.3 the transition mechanisms for two-dimensional boundary layers are discussed while Sections 5.3 to 5.5 relate to transition in three-dimensional boundary layers, with particular emphasis on transition in the flow over a swept wing.

5.1 Boundary-Layer Instability – Tollmien-Schlichting Waves

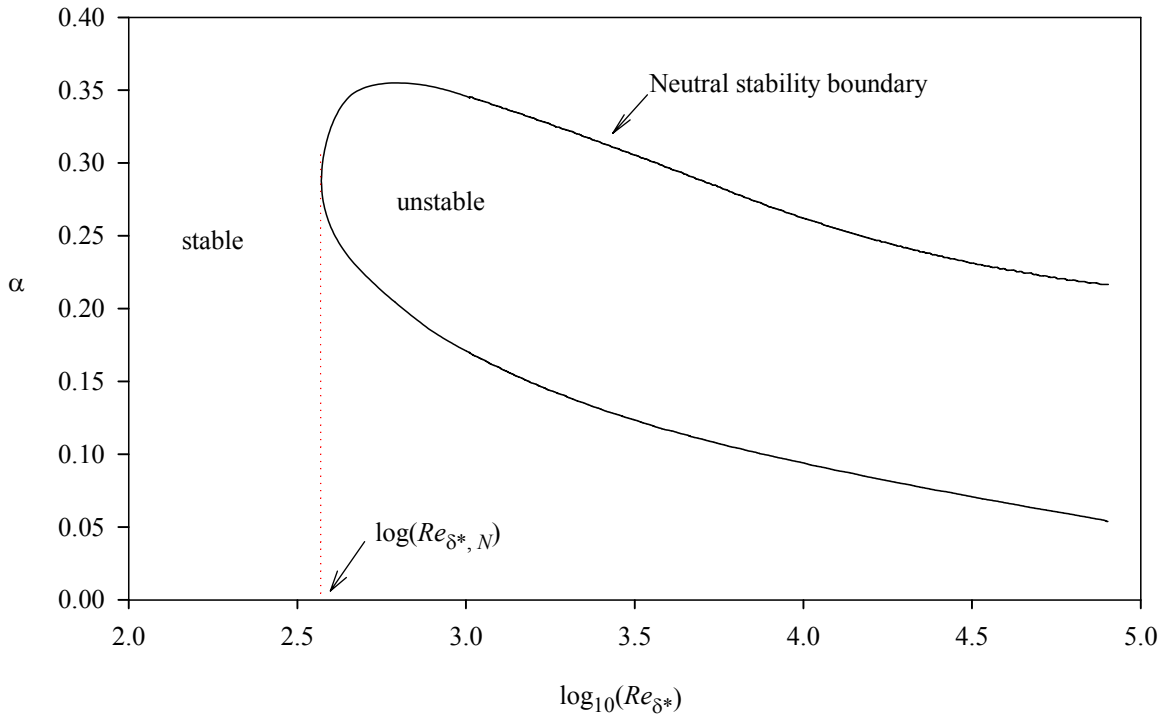

Sketch 5.1 Stability of boundary layer on a flat plate for disturbances having a range of non-dimensional wave number, α (derived from Reference 7)

For a two-dimensional boundary layer on a smooth flat plate, theoretical analysis[7,8] shows that small sinusoidal disturbances (known as Tollmien-Schlichting waves) are amplified, at some wave numbers α, if the Reynolds number is above a critical value, ($Re_{\delta*} \approx 500$) (Sketch 5.1). The results shown in Sketch 5.1 are derived using the Orr-Sommerfeld equation[7], which defines the stability criterion for small disturbances. The growth of these disturbances with time, at a fixed location, is examined (temporal analysis) as this simplifies the analysis. A similar result is obtained if the development of disturbances in the downstream direction is analysed for a flow with steady mean characteristics (spatial analysis).

5.1.1 Development and prediction of transition

When stability is neutral, the boundary layer does not become turbulent immediately. Further downstream the Tollmien-Schlichting waves distort progressively and turbulent spots appear, which coalesce in the transition region to form fully turbulent flow (G to H in Sketch 5.2).

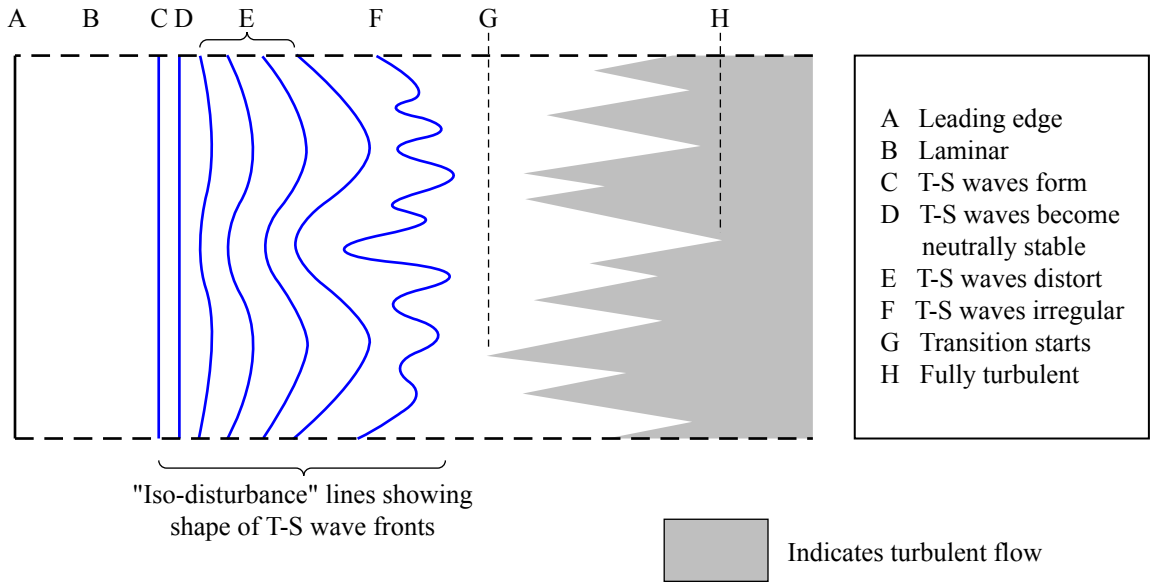

Note: The geometric form of the T-S wave distortion (D to F) and the turbulent breakdown (G to H) vary with time.

Sketch 5.2 Development of transition from Tollmien-Schlichting (T-S) instability (derived from Reference 7)

If the extent of the transition region is small, the transition position, at which the boundary layer becomes fully turbulent, may be estimated by the use of simple empirical correlations. One example is the empirical method due to Michel[9], which was obtained using a correlation between the Reynolds number based on the boundary-layer momentum-thickness at transition, $Re_{\theta,T}$, and that based on distance from the stagnation point $Re_{s_{stag}}$:

$$Re_{\theta,T} = 1.174\left(1 + \frac{2400}{Re_{s_{stag}}}\right) Re_{s_{stag}}^{0.46}. \tag{5.1}$$

This correlation has been shown to work well for a number of aerofoils but its performance in compressible flows is uncertain.

An alternative method that is commonly used to predict the onset of transition due to Tollmien-Schlichting waves is linear stability analysis combined with the e^N method[10,11], in which it is assumed that the amplitude of the waves increases with $(x - x_N)$ as:

$$\frac{A}{A_N} = e^N. \tag{5.2}$$

The variation of N with Reynolds number, for different wave numbers, can be derived using the Orr-Sommerfeld equation and the envelope to these curves is plotted on Sketch 5.3.

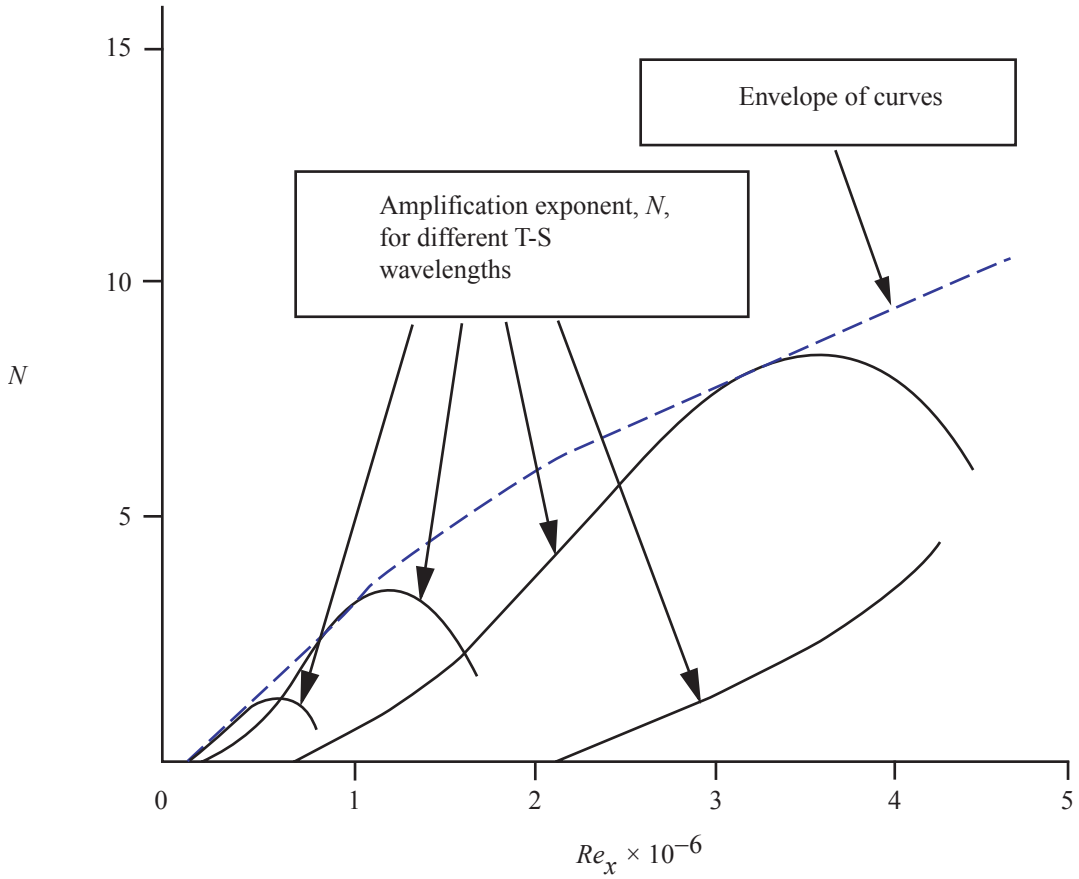

Sketch 5.3 Tollmien-Schlichting wave amplification (from Reference 7)

Correlation with wind-tunnel tests suggests that the start of transition corresponds to a value of N between 6 and 10, while fully turbulent flow corresponds to a somewhat higher value of N. If the extent of the transition region is small, a value of $N = 10$ is generally assumed. Since these values are sensitive to features of the flow environment such as turbulence and noise levels, they are likely to be significantly higher under full-scale flight conditions.

5.1.2 Pressure gradient

Transition is also affected by the surface pressure gradient in the flow. Sketch 5.4, shows the effect of pressure gradient expressed in terms of velocity gradient at the edge of the boundary layer on the Reynolds number for neutral Tollmien-Schlichting stability $(Re_{\delta^*,N})$, derived theoretically for the flow over a smooth flat plate with an imposed pressure gradient.

In Sketch 5.4, $\frac{\delta^2}{\nu}\frac{du_\delta}{dx}$ is used rather than pressure gradient itself. A positive value of this parameter corresponds to a negative pressure gradient in the x direction.

A positive pressure gradient in the direction of the flow promotes transition, while a negative pressure gradient delays it. It is seen from Sketch 5.4 that Tollmien-Schlicting waves can be stable in an "unfavourable" velocity gradient at low Reynolds number.

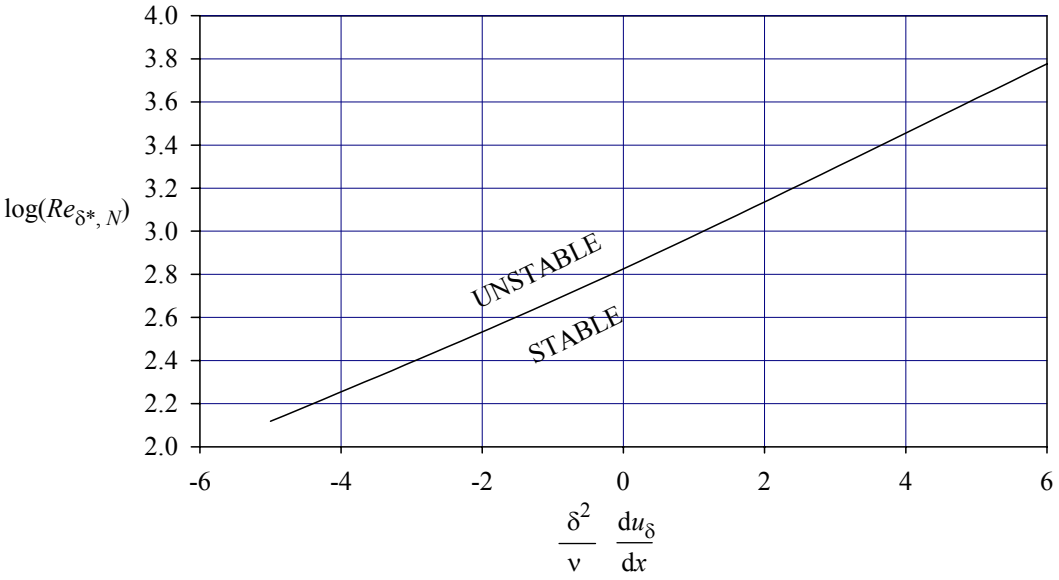

Sketch 5.4 Variation of neutral stability Reynolds number with velocity gradient parameter (derived from Figure 5.3 of Reference 7)

Granville[12] developed an empirical relationship for the lag between the neutral-stability location and the development of a fully turbulent boundary layer in terms of a pressure-gradient parameter (Sketch 5.5). This correlation is based on tests made on a variety of wing sections, both in flight and in low-turbulence wind tunnels.

Because the "average pressure gradient parameter", $\left(\frac{\theta^2}{\nu}\frac{d\bar{u}_\delta}{dx}\right)_{mean\ N\ to\ T}$ used in Sketch 5.5, is a mean value between the neutral-stability location and transition, an iterative approach is required to make use of it in order to estimate transition location. Also, the pressure distribution around an object is sensitive to transition and boundary-layer growth. Thus, when using the methods illustrated in Sketch 5.4 and Sketch 5.5 to estimate transition location, further iteration may be required to update the assumed surface pressure distribution at each step.

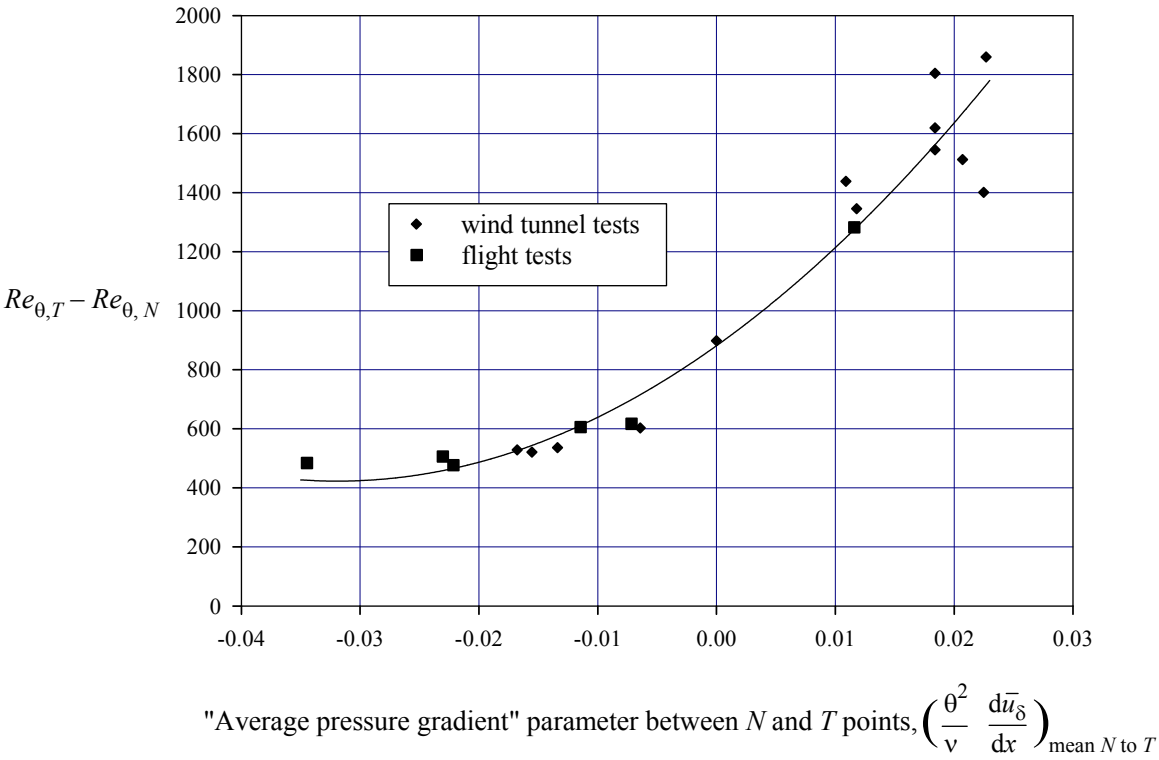

Sketch 5.5 Difference between transition and neutral stability Reynolds numbers (derived from Reference 12)

5.1.3 Freestream turbulence and noise-receptivity

The transition process is influenced by the levels of turbulence and noise in the freestream. These disturbances are transmitted to the boundary layer from outside, a process known as "receptivity". Transition is influenced by the frequency spectrum of such disturbances. Their effects may be accentuated by coupling to natural periodicity within the boundary layer itself, such as wall waviness, distributed surface roughness, steps and gaps, *etc*.

Generally, however, freestream turbulence and acoustic disturbances are of longer wavelength than those typical of boundary-layer disturbances[13]. Goldstein[14,15] and Goldstein, Leib and Cowley[16] show that energy transfer of the freestream disturbances into the boundary layer is strongest in regions where the boundary layer is thin and has a high rate of growth. These conditions are likely to be met near the leading edge of an aerofoil.

Bertolotti and Crouch[17] proposed a theoretical prediction method for the effects of a simple disturbance. Experimental studies, *e.g.* Wiegel and Wlezien[18] and numerous theoretical studies, *e.g.* Crouch[19], are also available but, as yet, there is no comprehensive prediction method for the effect of receptivity on transition.

Dryden[20] gives details of experiments on a flat plate at zero incidence and provides a correlation between the transition Reynolds number, $(Re_T = (U_\infty x_T)/\nu)$ and the non-dimensional freestream turbulence intensity, $\left(T_\delta = \left(\overline{u'^2} + \overline{v'^2} + \overline{w'^2}\right)^{1/2} \Big/ (3u_\delta)\right)$.

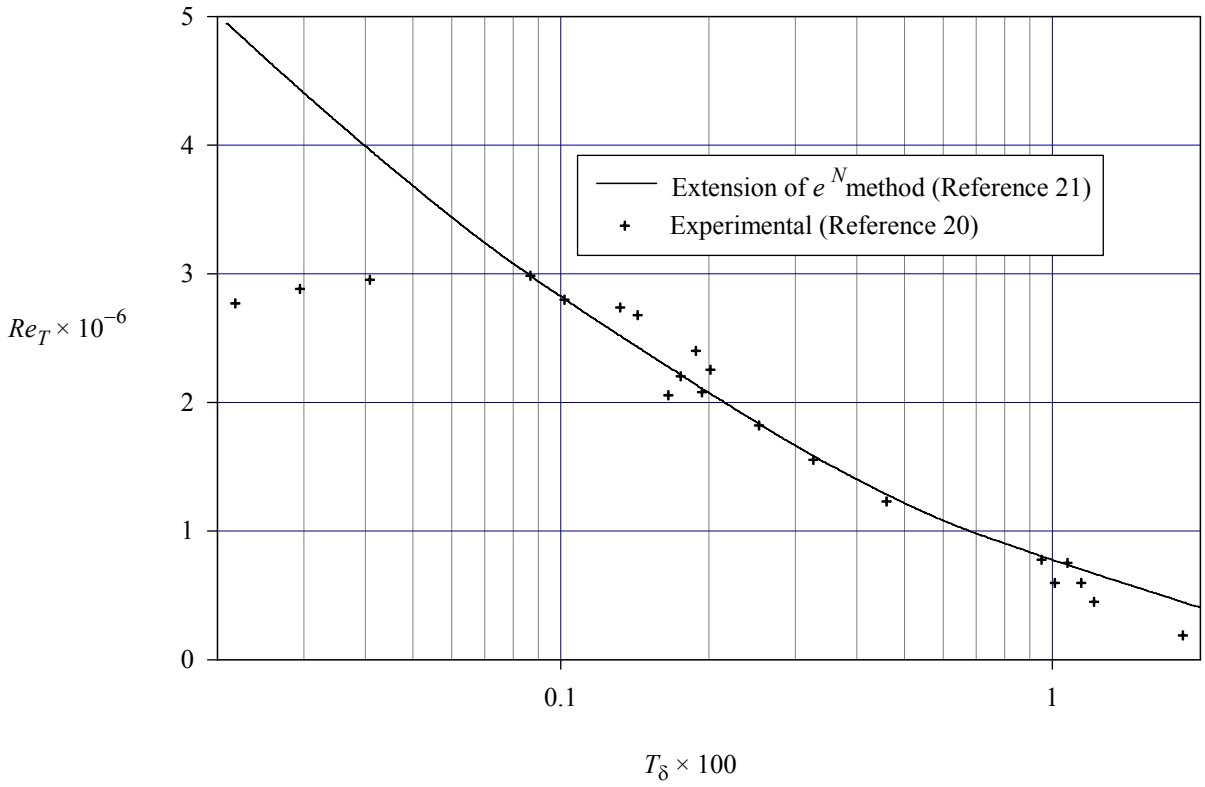

Sketch 5.6 Effect of freestream turbulence on transition Reynolds number for a flat plate (from Reference 7)

Sketch 5.6 shows that the transition Reynolds number is not affected by freestream turbulence if T_δ is less than approximately 0.001. An extension to the e^N method, to predict the effect of freestream turbulence, is given by Mack[21]. This uses a correlation of the empirical results of Dryden[20] to give the variation of N with freestream turbulence in the form:

$$N = -8.34 - 2.4 \ln T_\delta \,. \tag{5.3}$$

Mack's curve is shown in Sketch 5.6. Van Ingen[10] gives similar correlations for the values of N defining the start and end of the transition region:

$$N = 2.13 - 6.18(\ln T_\delta) \text{ (start)}, \tag{5.4}$$

$$N = 5.0 - 6.18(\ln T_\delta) \text{ (end)}. \tag{5.5}$$

5.1.4 Surface roughness

Below a given excrescence (*i.e.* roughness element) height, e_{crit1}, naturally-occurring distributed roughness has no effect on boundary layer transition. Schiller[22] argues that this height is related to the onset of a vortex street, associated with an individual surface excrescence, which destabilises the boundary-layer flow. Thus e_{crit1} depends on the local excrescence Reynolds number $Re_e (= u_e e/\nu)$.

The critical value, $Re_{e_{crit1}}$, depends on the 'aspect ratio' of the excrescences[23], as shown in Sketch 5.7. This sketch shows a large range for the parameter d_e/e and, at the higher end of the scale, excrescences are essentially two-dimensional protuberances, normal to the flow direction. In this case, transition is no longer effected by the shedding of a vortex street from the protuberance. Instead, the disturbance directly influences the Tollmien-Schlichting stability. Surface waviness has a similar destabilising effect.

The relationship between $Re_{e_{crit1}}$ and d_e/e appears to be independent of compressibility (below a Mach number of approximately 3)[23]. It is also independent of the local external pressure gradient[23,24]. It is important to note, however, that a normally favourable pressure gradient may be destabilising in the presence of roughness. This is because any thinning of the boundary layer, caused by the favourable pressure gradient, increases u_e and hence Re_e, at a given roughness height. In the case of protuberances having high d_e/e, producing nearly two-dimensional disturbances that affect Tollmien-Schlichting stability, this increase in Re_e will be offset by the stabilising effects discussed in Section 5.1.2.

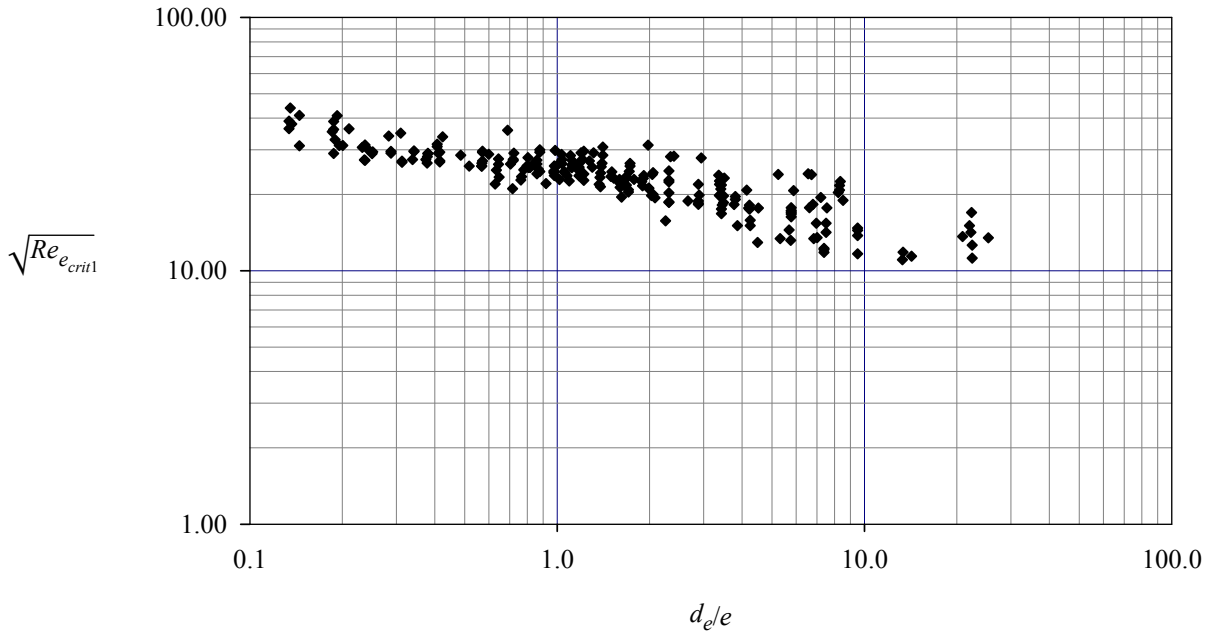

Sketch 5.7 Variation of $Re_{e_{crit1}}$ with 'aspect ratio' of element of distributed roughness (from Reference 23)

The value of Re_e at any location is related to the local laminar-boundary layer conditions. Assume a sine velocity profile, $u/u_\delta = \sin(\pi z/2\delta)$ in the boundary layer over a flat plate, located in the plane $z = 0$, with zero pressure gradient and with the flow in the x direction. The variation of Re_e with $Re_{xe} = u_\delta x_e/\nu$ and $Re_{\delta e}/(u_\delta e/\nu)$ is given[7] by:

$$Re_e = Re_{\delta e} \sin\left(\frac{\pi}{10} Re_{\delta e} Re_{xe}^{-1/2}\right). \tag{5.6}$$

This function is shown in Sketch 5.8.

A correlation of the data in Sketch 5.7 enables $Re_{e_{crit1}}$ to be found if d_e/e is known. $Re_{\delta e}$ may then be determined, for the appropriate value of Re_{xe}, using Sketch 5.8. Since in any particular flow u_δ and ν are known, the critical excrescence height, e_{crit1}, may then be calculated.

If the pressure gradient is not zero, an equivalent relationship to Equation (5.6) may be obtained by solution of the integral boundary layer equations[7].

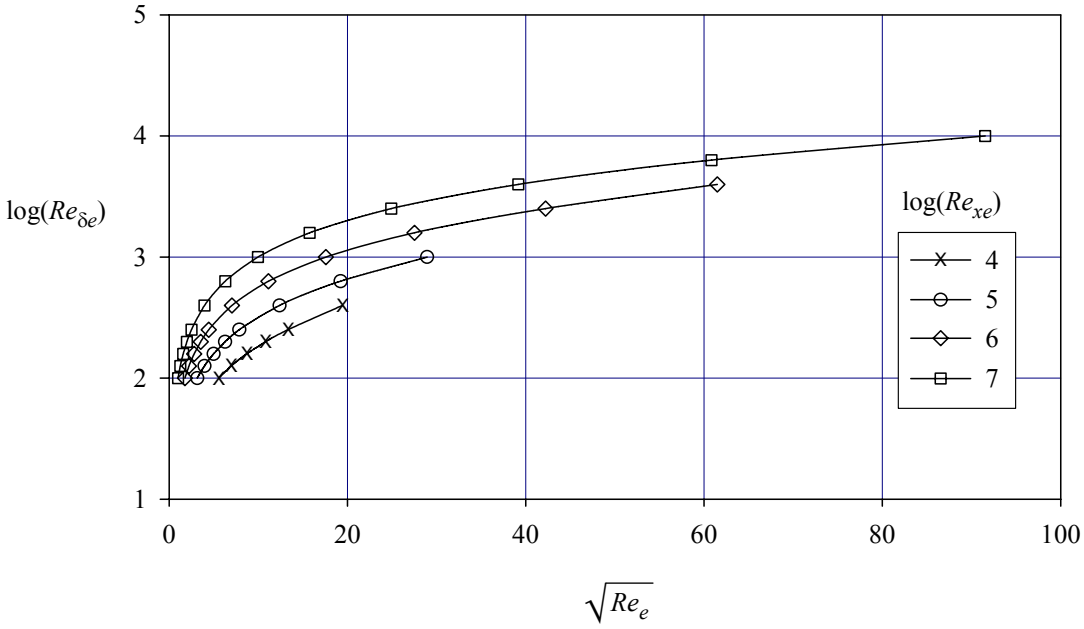

Sketch 5.8 Relationship between excrescence Reynolds numbers for sine velocity profile

Disturbances in the boundary layer generated by an excrescence of height, e_{crit1}, take some distance to amplify and the onset of turbulent flow moves upstream towards the originating excrescence as e is increased above e_{crit1}. The onset of turbulent flow effectively occurs at the excrescence when e reaches a second critical value, e_{crit2}.

Van Driest and Blumer[25] give the following empirical relationship based on tests on bands of spherical roughness with zero external pressure gradient:

$$\frac{u_\delta e_{crit2}}{\nu} = 42.6 Re_{xe}\left[1 + \frac{1}{2}(\gamma - 1)M_\delta^2\right]. \qquad (5.7)$$

This applies at both subsonic and supersonic speeds.

For tests in high Reynolds number wind tunnel facilities, with natural transition, the effect of surface roughness is very significant and a very smooth model surface finish is generally required because transition induced by surface roughness may lead to a pseudo Reynolds number effect (Section 8.3.4).

5.2 Concave Surface Curvature – Görtler Vortices

If concave surface curvature is present, a further flow mechanism is introduced, in laminar flow, with the formation of Görtler vortices[7,26] (Sketch 5.9). Görtler[26] shows, theoretically, that these vortices appear when

$$\frac{u_\delta \theta}{\nu}\sqrt{\frac{\theta}{|r_0|}} > 0.58\,. \qquad (5.8)$$

Liepmann[27] shows by experiment that the regular structure of the vortices breaks down when

$$\frac{u_\delta \theta}{\nu}\sqrt{\frac{\theta}{|r_0|}} > 7.3\,, \tag{5.9}$$

resulting in transition to fully turbulent flow.

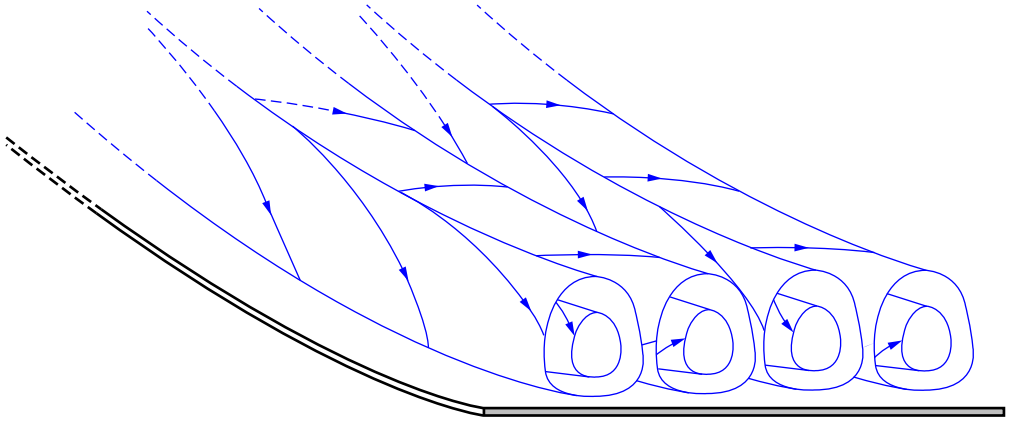

Sketch 5.9 Görtler vortices on concave surface (from Reference 13)

5.3 Cross-flow Instability

The boundary layer stability on swept wings is influenced by the velocity component parallel to the wing leading edge. The pressure distribution over the wing, outside the boundary layer, causes changes in the velocity component normal to the leading edge. These modify the local flow direction, causing the streamlines to curve (Sketch 5.10). This curvature is associated with a pressure gradient parallel to the surface and normal to the local streamline direction.

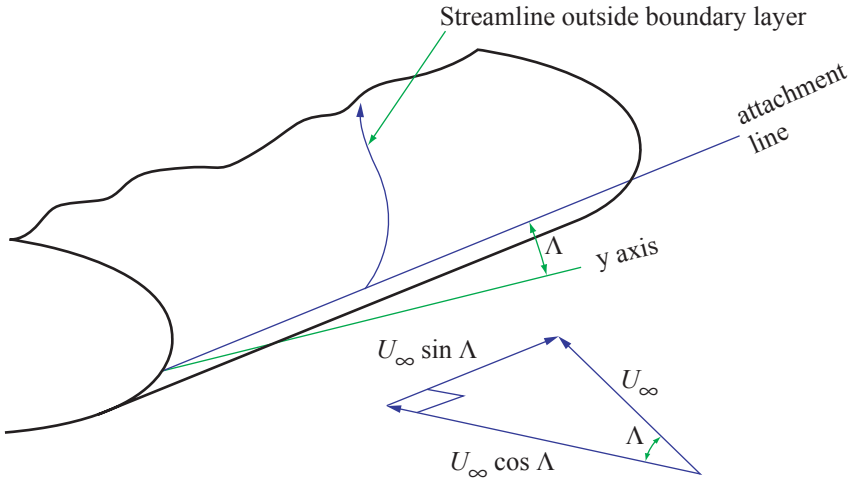

Freestream velocity normal to y axis = U_∞
Velocity component parallel to leading edge = $U_\infty \sin \Lambda$
Velocity component normal to leading edge = $U_\infty \cos \Lambda$

Sketch 5.10 Curvature of streamlines due to spanwise velocity component

This pressure gradient causes the development of a cross-flow velocity profile, within the boundary layer, in a direction normal to the external streamline. Because of the no-slip condition at the wing surface, the cross-flow velocity will be zero at the wing surface as well as at a streamline external to the boundary layer. (Sketch 5.11).

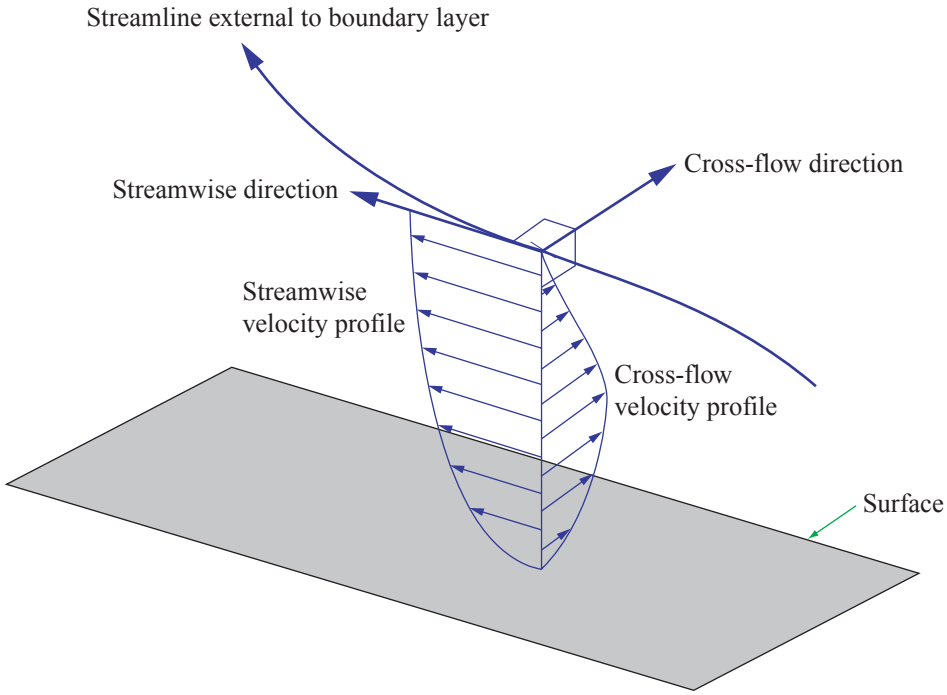

Sketch 5.11 Cross-flow and streamwise velocity profiles in boundry layer

These changes of direction, within the boundary layer, if sufficiently severe, lead to the production of vortices (Sketch 5.12) and consequent boundary layer transition.

The presence of a favourable pressure gradient, from the point of view of delaying Tollmien-Schlichting instability (Section 5.1), has a detrimental effect on the cross-flow stability.

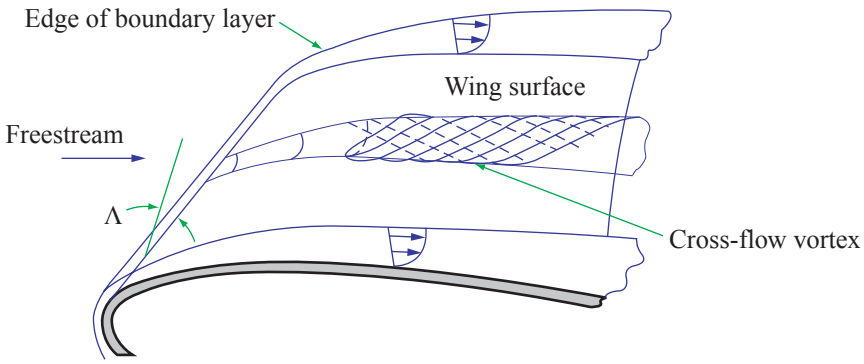

Sketch 5.12 Vortices generated by cross flow on swept wing (derived from Reference 16)

Sketch 5.13 shows the variation of transition location with sweep angle for a symmetric section wing of 15% thickness and constant chord with the maximum thickness at 40% chord[28]. Transition was detected using the china-clay visualisation technique[29] and tests were made at zero incidence at low Mach number.

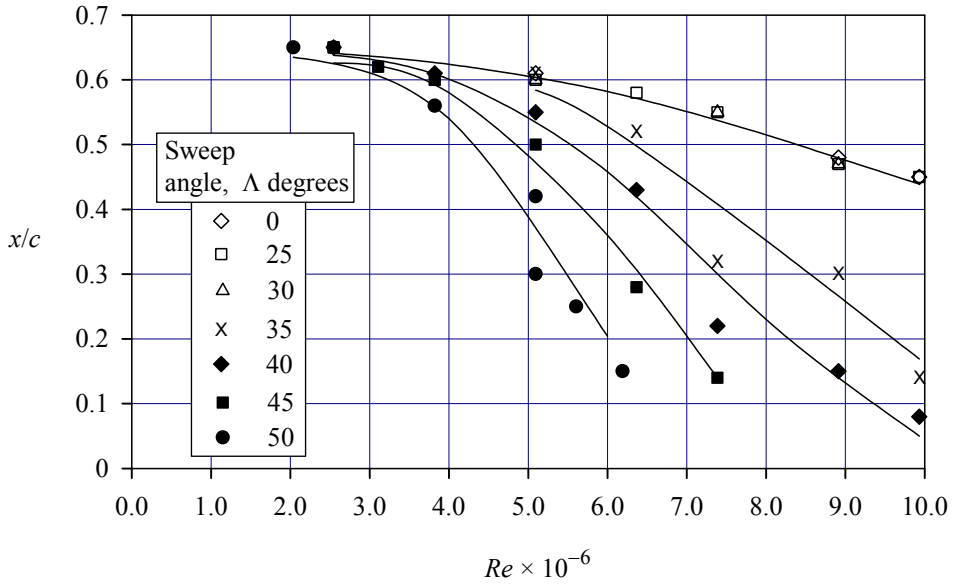

Sketch 5.13 Effect of sweep angle on the transition location on a symmetric section wing at zero incidence (derived from Reference 28)

It can be seen that there appears to be no effect of sweep until the sweep angle exceeds 30 deg. After this, the onset of cross-flow instability causes the formation of cross-flow vortices (observation of which is also reported in Reference 28) and early transition to turbulent flow.

The data given in Reference 28 are of limited value in predicting the transition on a general wing section, as the cross-flow velocity profile depends on the detailed pressure distribution over the swept wing. Currently, most practical transition prediction methods for cross-flow instability depend on an extension of the e^N method. Examples of such methods are the C1 and C2 methods described by Arnal, Habiballah and Coustols[30]. These methods involve correlation of N with local boundary-layer characteristics and, in the case of the C2 method, the freestream turbulence.

White, *et al.*[31] point out that a fundamental difference between Tollmien-Schlichting instability and cross-flow instability is that the former involves travelling disturbances while, in the latter case, the cross-flow vortices have a fixed location. Because of this, the amplification of the two types of disturbance differs in nature and this leads to problems in the application of the e^N method in the case of the fixed disturbance, where nonlinear effects are often of great significance. In this case the use of a nonlinear technique, such as the nonlinear parabolised stability equation (NPSE),[32, 33] is more appropriate.

5.4 Leading-edge Contamination

The spanwise flow component along the attachment line at the leading-edge of the wing causes boundary layer growth along the region of the leading-edge in the spanwise direction. Transition may occur due to this boundary layer development and is influenced by turbulent flow emanating from the wing-fuselage junction and surface imperfections along the leading edge. Once turbulence has been established in this region of the boundary layer it spreads over the wing surface and is thus known as leading-edge contamination.

Young[7] suggests a simple criterion for the presence of leading-edge contamination. If the Reynolds number, based on the spanwise velocity along the leading edge and the boundary layer momentum thickness, exceeds approximately 250, then leading-edge contamination is possible in the presence of a sufficiently strong disturbance.

Pfenniger[34] gives an alternative empirical criterion, which relates the leading-edge geometry and the freestream flow properties to the presence of leading edge contamination. This criterion implies that leading-edge contamination is not present if:

$$Re_{\theta\ attachment\ line} \approx \frac{\sin\Lambda}{\sqrt{\cos\Lambda}}\sqrt{\frac{\rho_\infty U_\infty r_{l.e.}}{\mu_\infty(1+\tau_{ell})}} < 90\,, \tag{5.10}$$

(where $r_{l.e.}$ is the leading-edge radius, measured normal to the leading edge, and τ_{ell} is the thickness ratio of the ellipse which best fits the wing section shape at the leading edge).

5.5 Summary of Mechanisms and Factors which may Influence Transition on a Swept Wing

Prediction of transition in three-dimensional flows, such as the flow over a swept wing, is complicated by the fact that there are a number of possible transition mechanisms:

(a) Leading-edge contamination,

(b) Cross-flow instability,

(c) Görtler vortex formation,

(d) Tollmien-Schlichting wave amplification.

All these mechanisms need to be assessed, as the particular mechanism which eventually causes transition may not be obvious *a priori*.

Tollmien-Schlichting instability involves travelling disturbances, which are driven primarily by turbulence receptivity while the fixed disturbances in cross-flow instability are driven mainly by surface irregularities.[31] Thus the transition mechanism which is dominant in a particular case depends on both the freestream turbulence and the surface roughness. Experimental work by Deyhle and Bippes[35] showed that Tollmien-Schlichting waves dominate if the freestream turbulence intensity, T_u, exceeds approximately 0.0015.

Sketch 5.14 gives a simplified sequence for implementation showing the various transition mechanisms that should be considered in the determination of swept-wing transition. Sketch 5.15 indicates how suitable estimation methods for each mechanism may be selected.

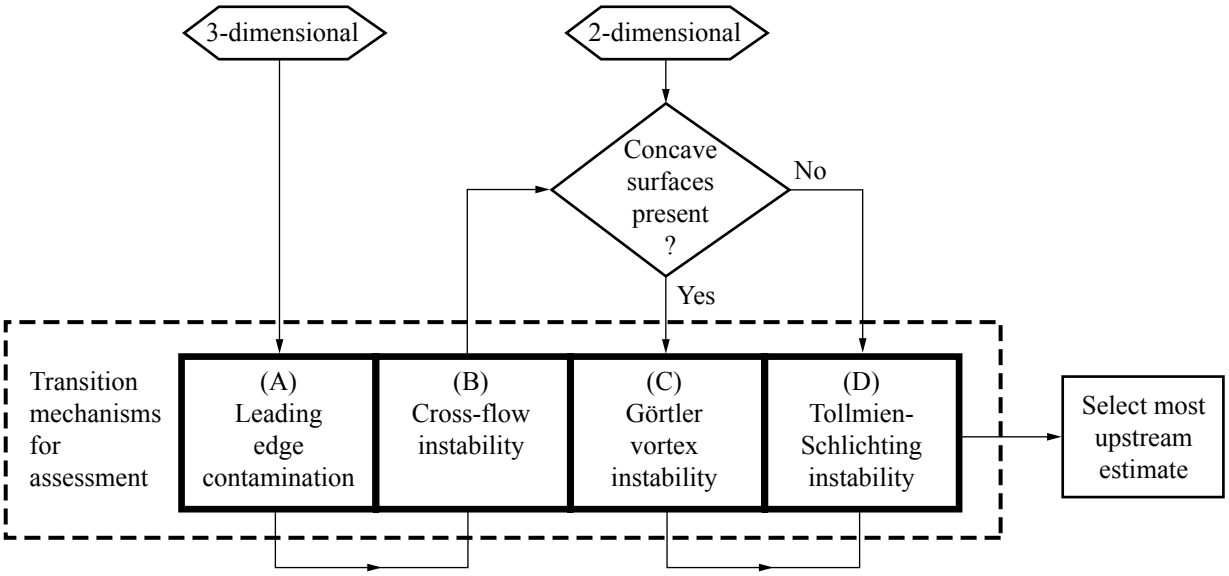

Sketch 5.14 Implementation sequence for transition mechanisms (A) to (D)

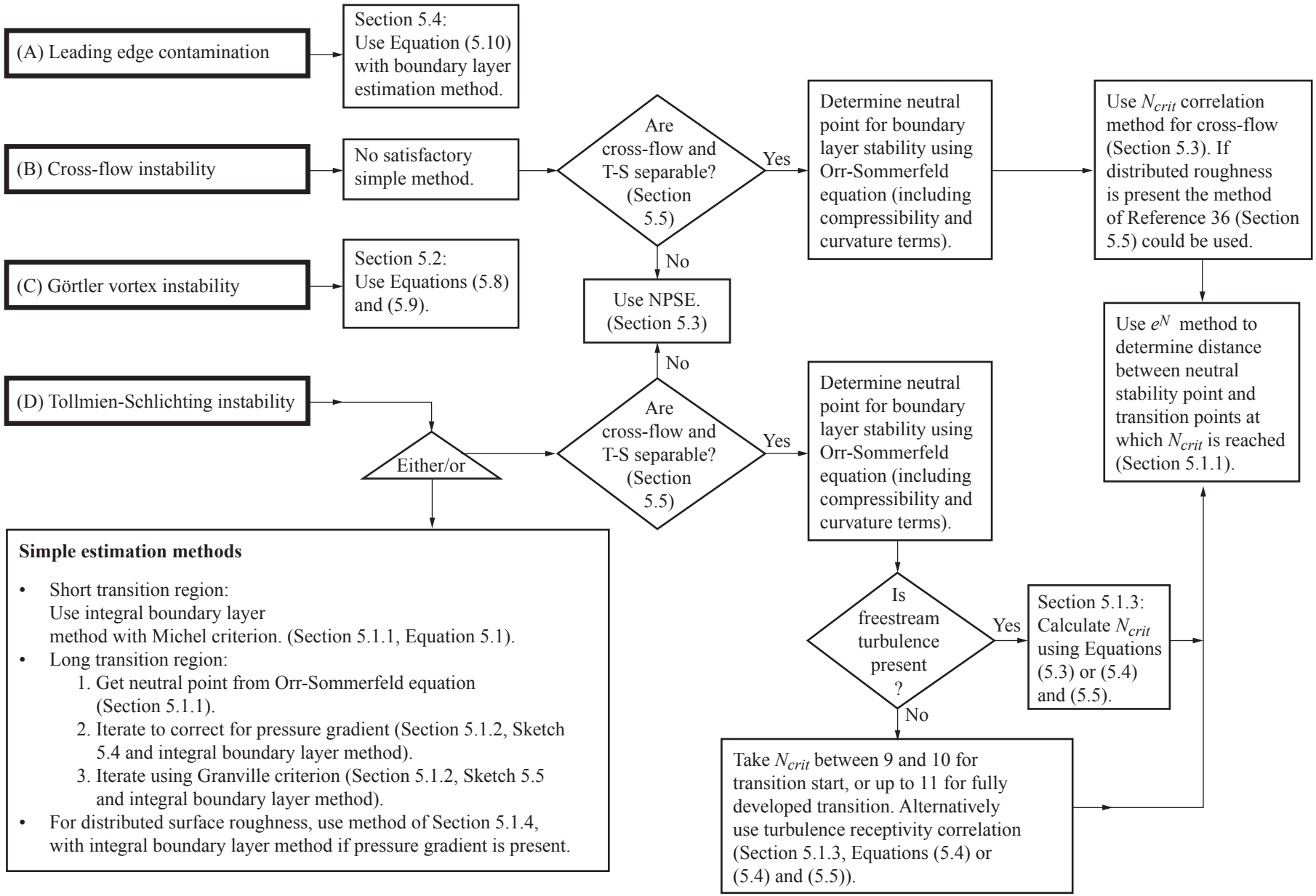

Sketch 5.15 Detailed treatment of transition mechanisms (A) to (D)

As indicated in Sketch 5.15, transition on swept wings, caused by Tollmein-Schlichting or cross-flow instability, may be assessed using the e^N method (Section 5.1.1). Here the neutral stability point is evaluated from the Orr-Sommerfeld stability equation (Section 5.1), which may be modified to include both compressibility and curvature terms. The distance between the neutral stability point and the transition location is then determined by using the Orr-Sommerfeld equation to calculate the distance required to attain an empirical critical value of the amplification factor, N.

The success of this method in the prediction of Tollmien-Schlichting instability is, at least in part, due to the fact that the empirically determined critical value of N already includes the influence of such factors as the effect of non-linearities in the breakdown to turbulence and the mechanism which excites the disturbance, such as freestream turbulence or acoustic waves.

When cross-flow instability occurs, transition is caused by the presence of stationary, rather than moving disturbances[31]. Thus, although the e^N method is commonly used for transition prediction on swept wings, it does not reflect the physics of cross-flow transition, and is unlikely to provide a satisfactory tool for the accurate prediction of transition in these circumstances. However, empirically modified e^N methods, such as that proposed by Crouch and Ng[36], employing correlations of N with surface roughness, give useful guidance.

In some cases the Tollmien-Schlichting and cross-flow mechanisms may be excited simultaneously and mutual interaction then takes place. In this case, the e^N method is unlikely to give satisfactory results because the interaction between the two mechanisms is non-linear. In this case transition is difficult to predict, although some guidance may be obtained by the use of the NPSE method (Section 5.3). Also, the decision as to the separability of the two mechanisms (Sketch 5.15) is likely to be difficult, unless considerable experience is available for wing geometries close to that under investigation. In the absence of this experience, it is possible to apply the e^N method to both mechanisms individually and compare the results to see if the predicted transition locations differ widely. If they do, the mechanisms are likely to be uncoupled.

Sketch 5.16 indicates (as an approximate boundary) the Reynolds numbers below which it may be possible to achieve a substantial region of laminar flow on the wing of an aircraft by appropriate geometric shaping and attention to surface finish. These Reynolds numbers decrease with increasing leading edge sweep. At moderate sweep angle, cross-flow instability is likely to be the dominant transition mechanism while, at greater sweep angle, leading-edge contamination is the primary influence. A second boundary is also shown to indicate the extent to which suction and attention to surface profile and finish may be used to delay the transition process.

For wings with significant sweep, full-scale transition is most likely to occur close to the leading edge and be caused by leading edge contamination (Sketch 5.16), although this may not be so for a model test conducted at a low Reynolds number. In this case it is necessary to fix artificially the transition location in the wind tunnel by, for example, the use of a band of surface roughness[37] (see also Section 5.1.4). In this case, correction of the wind-tunnel model results is still required, since the boundary layer characteristics are not representative of the full-scale flow. Because of the need to model the interaction between the boundary layer and any shock waves formed in transonic flow (Section 6.2), simply fixing the model transition location, so that it coincides with the full-scale case, is not adequate and a complex strategy is required to provide sufficient data to allow adequate interpretation of wind-tunnel results[38].

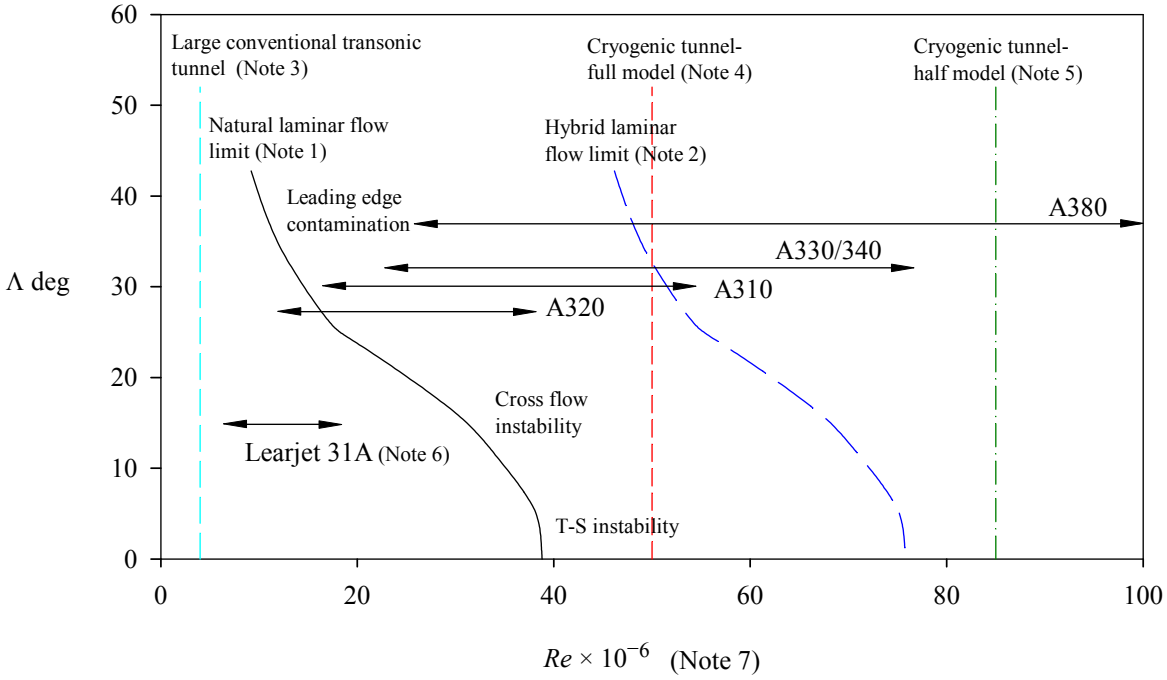

Note 1 Boundary representing the Reynolds number below which it may be possible to achieve significant areas of laminar flow by profile shaping and attention to surface finish. Likely transition mechanisms are indicated for different wing sweep angles.

Note 2 Boundary representing the Reynolds number below which it may be possible to achieve significant areas of laminar flow by the use of suction, in addition to surface shaping and attention to surface finish.

Note 3 Vertical line representing the Reynolds number of a test on a half-model transport aircraft, of 1.4 m semi-span, in a large conventional transonic tunnel at $M_\infty = 0.8$ (ambient stagnation pressure).

Note 4 Vertical line representing the maximum achievable Reynolds number for a complete aircraft model, at typical cruise Mach number, in a large cryogenic transonic wind tunnel (Reference 39).

Note 5 Vertical line representing representing the maximum achievable Reynolds number, at typical cruise Mach number, for a half model in a large cryogenic transonic wind tunnel (Reference 39).

Note 6 Typical operating Reynolds number ranges for different aircraft types. It should be noted that, if the Reynolds number for a particular aircraft falls below the boundary described in Note 1, this does not imply that significant laminar flow is actually achieved on that aircraft since this depends on such factors as the section design.

Note 7 Reynolds numbers are based on mean chord.

Sketch 5.16 Variation of laminar flow boundaries with leading-edge sweep angle and probable transition mechanisms (derived from Reference 39)

Sketch 5.16 indicates that it may be possible to obtain substantial regions of laminar flow over the wing of a small aircraft with low sweep, or where suction is used to delay transition. Where this is the case, the full-scale transition point is unknown *a priori* and, even for a wind tunnel-test at full-scale Reynolds number, the transition mechanism may be influenced by the quality of the airflow and the acoustic environment within the tunnel.

6. BOUNDARY-LAYER SEPARATION

In addition to its influence on the transition of the boundary layer from laminar to turbulent flow, Reynolds number also influences the separation behaviour of the boundary layer. Separation is of particular significance in transonic flows where shock-induced separation can occur. For this reason, the mechanisms involved in boundary-layer separation are briefly discussed here.

An adverse pressure gradient (positive in the direction of the velocity at the edge of the boundary layer) is accompanied by a distortion of the velocity profile in the z direction. Progressive distortion of the velocity profile leads to a flow reversal near the surface (Sketch 6.1).

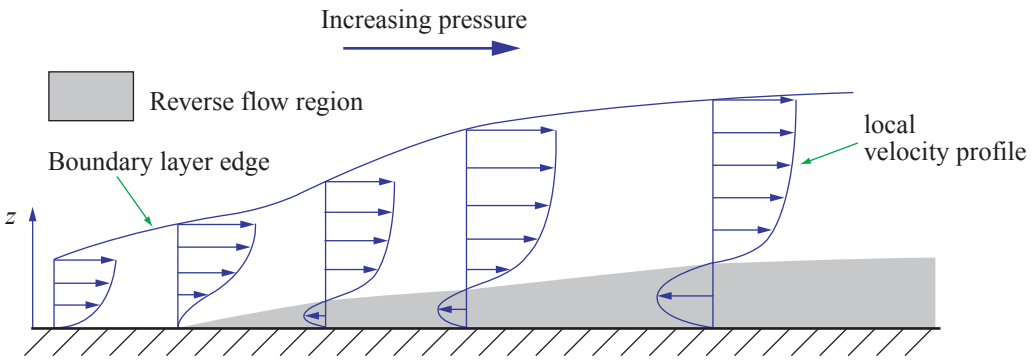

Sketch 6.1 Development of reverse flow due to adverse pressure gradient

Separation is indicated by the presence of this reverse flow region and an associated displacement of the edge of the boundary layer away from the surface. Separation of both laminar and turbulent boundary layers can occur. However, separation takes place more readily when the boundary layer is laminar. This is because the turbulent mixing process, in a turbulent boundary layer, restricts the distortion of the velocity profile and thus delays the formation of the reverse flow region.

Stratford[29] developed the simple criterion that, at the separation location of a two-dimensional laminar boundary layer in incompressible flow:

$$x_{pg}^2 C_p \left(\frac{\mathrm{d}C_p}{\mathrm{d}x} \right)^2 = \text{constant} . \qquad (6.1)$$

Curle and Skan[41] suggested a value of 0.0104 for the constant in Equation (6.1). This criterion assumes the existence of an undisturbed region at constant pressure upstream of the pressure gradient. The distance x_{pg} is the distance from the beginning of the adverse pressure gradient to the separation location.

References 42 and 43 describe a method for predicting the separation boundary* in transonic flow, with a turbulent boundary layer.

* Conditions under which the effects of separation first become significant, in some specified way.

Separation is associated with a number of different forms and causes, as described below.

6.1 Seperated Flow Types in the Absence of Shock Waves

Following separation a wake may form, as shown for example in Sketch 6.2. Alternatively separation may be followed by reattachment to the surface, forming a separation bubble (Sketch 6.3). Following reattachment, the boundary layer may remain in its initial state, giving either a laminar (*e.g.* Reference 44) or a turbulent separation bubble.

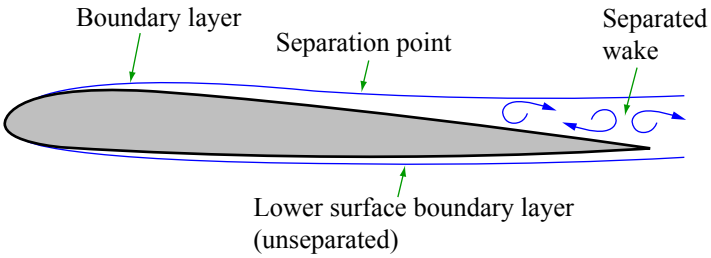

Sketch 6.2 Wake formation due to boundary layer separation on upper surface

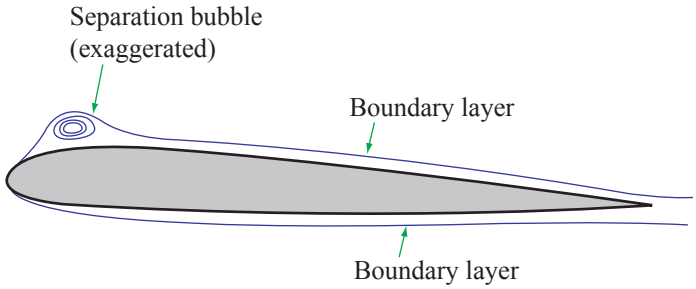

Sketch 6.3 Formation of separation bubble followed by boundary layer reattachment (schematic)

Since laminar separation is destabilising, the flow within the separated shear layer usually becomes turbulent just downstream of the separation point. Turbulent mixing may then suppress the reversed flow and lead to reattachment even in the presence of an unfavourable pressure gradient (Sketch 6.4). A transition* separation bubble is then formed.

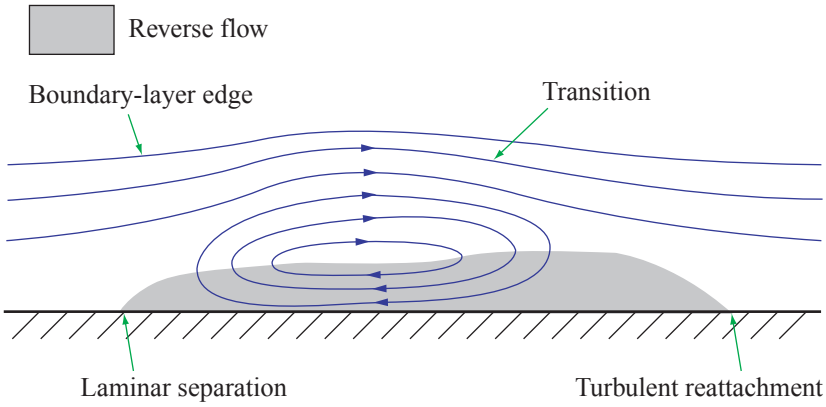

Sketch 6.4 Transition separation bubble

* Since laminar reattachment is uncommon, the term "laminar separation bubble" is often used in the literature instead of "transition separation bubble".

Sketch 6.5 shows the oil flow pattern produced by a transition separation bubble obtained experimentally on a two-dimensional aerofoil section.

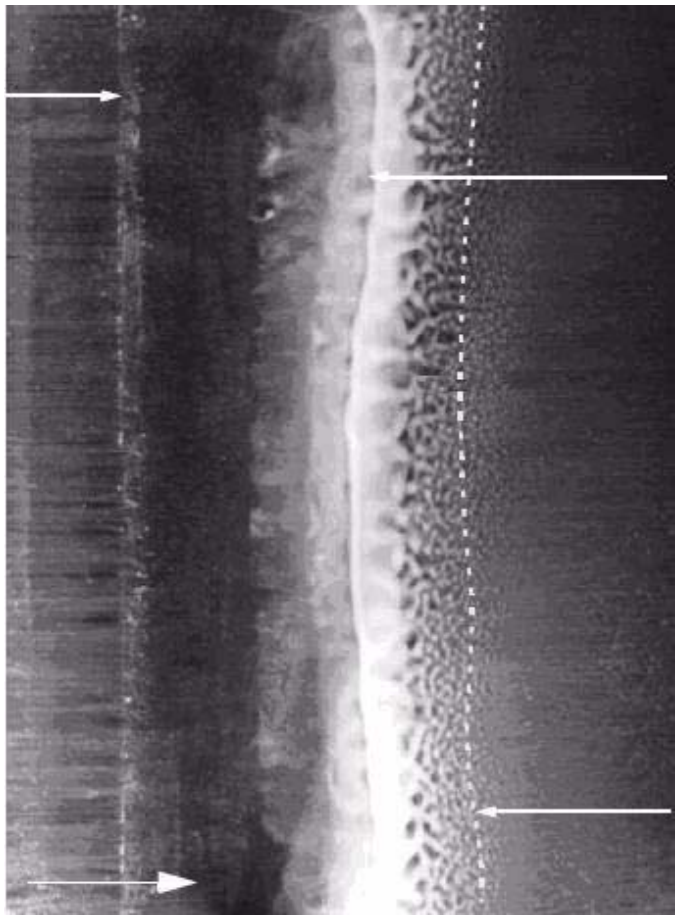

Sketch 6.5 Oil flow picture of transition separation bubble (derived from Reference 45)

6.2 Shock-Wave/Boundary-Layer Interaction

An extensive account of shock-wave/boundary-layer interaction phenomena is given by Delery and Marvin[46]. The increase of pressure across a shock wave may have a number of effects on the boundary layer:

Thickening of the layer,

Transition from a laminar to a turbulent boundary layer,

Separation of the boundary layer.

Interaction between a shock wave and a laminar boundary layer usually results in transition to turbulent flow. Separation may also take place and this may be extensive, or localised in the form of a transition bubble.

Pearcey[47] examined interaction between a shock wave and a locally turbulent boundary layer on aerofoils in transonic flow. He divided flows involving separation into two main categories, referred to as type A and type B.

In type A flows, the shock wave initially causes boundary layer thickening. As the shock strength increases with either M_∞ or α, a separation bubble forms at the foot of the shock wave and rapidly grows in extent as Mach number or incidence is further increased (Sketch 6.6). Type A flow occurs when there is a moderate adverse pressure gradient downstream of the shock wave.

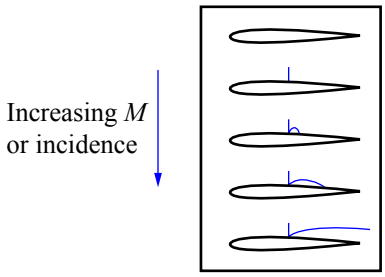

Sketch 6.6 Development of type A shock/boundary layer interaction

Type B flows typically occur when there is a strong recompression near the trailing edge. This is likely to occur when the point of maximum thickness on the aerofoil is well aft, with low curvature over much of the upper surface followed by a comparatively high curvature near the trailing edge. Type B flows are characterised by the presence of a separation near the trailing edge, which is either caused or exacerbated by the presence of the shock wave. Type B flows may be further sub-classified into cases where the trailing edge separation is provoked by perturbations caused by a shock-induced separation bubble, directly by the shock wave, or where the separation already exists in the absence of the shock but is exacerbated by shock wave development accompanying increasing Mach number or incidence (Sketch 6.7).

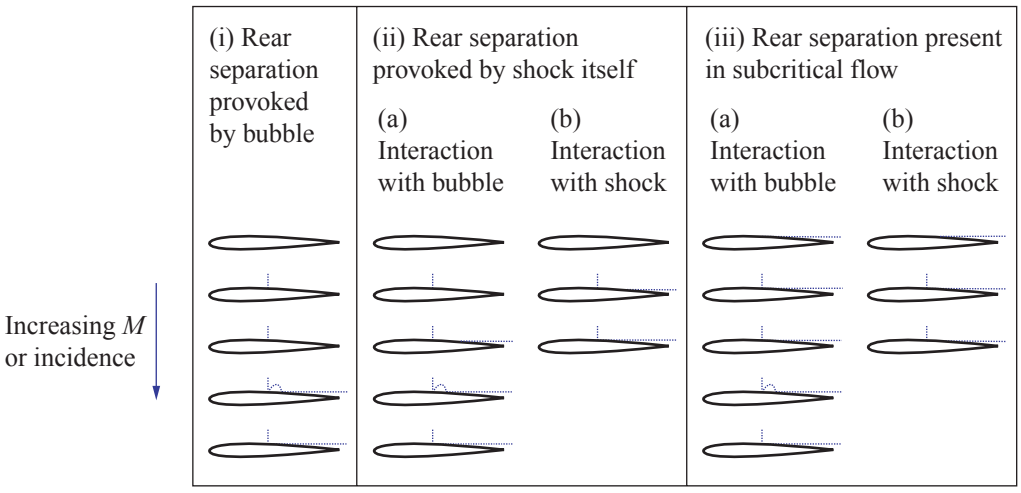

Sketch 6.7 Variants of type B shock/boundary layer interaction (Reference 47)

In type B(i) flows, increasing Mach number or incidence causes the formation of a shock wave. As the strength of the shock increases, a separation bubble appears at its foot. This disturbs the downstream boundary layer causing separation at the trailing edge of the aerofoil. As the Mach number or incidence is further increased, the separation point moves towards the shock until, eventually, the separated region covers the whole of the surface, downstream of the shock.

In type B(ii) flow, even in the absence of a separation bubble, the shock wave produces sufficient disturbance in the downstream boundary layer to cause separation at the trailing edge. Again, the extent of this separation increases with increasing Mach number or incidence, until it occupies the entire region downstream of the shock wave. After trailing-edge separation has initiated, a separation bubble may form at the foot of the shock wave (type Bii (a)), or the separation may develop without the formation of a bubble (type Bii (b)).

Trailing-edge separation develops prior to shock wave formation in type B (iii) flow. The formation of the shock, as Mach number or incidence increases, exacerbates the separation, which develops with increasing shock strength either with the formation of a separation bubble at the foot of the shock wave (type Biii (a)), or without the formation of a bubble (type Biii (b)).

As stated in Section 5, the transition location at full scale is likely to be close to the wing leading-edge. Consequently, at full scale, any shock-wave interaction is likely to occur with a turbulent boundary layer, resulting in one of the flow types described in this section.

Because of the sensitivity of shock-induced separation to the local boundary-layer state and the dependency of the boundary layer characteristics on Reynolds number, large discrepancies between the flow observed in a wind tunnel and that observed in flight[48] may occur, even where boundary-layer transition is fixed in the wind tunnel test. This is illustrated in Sketch 6.8.

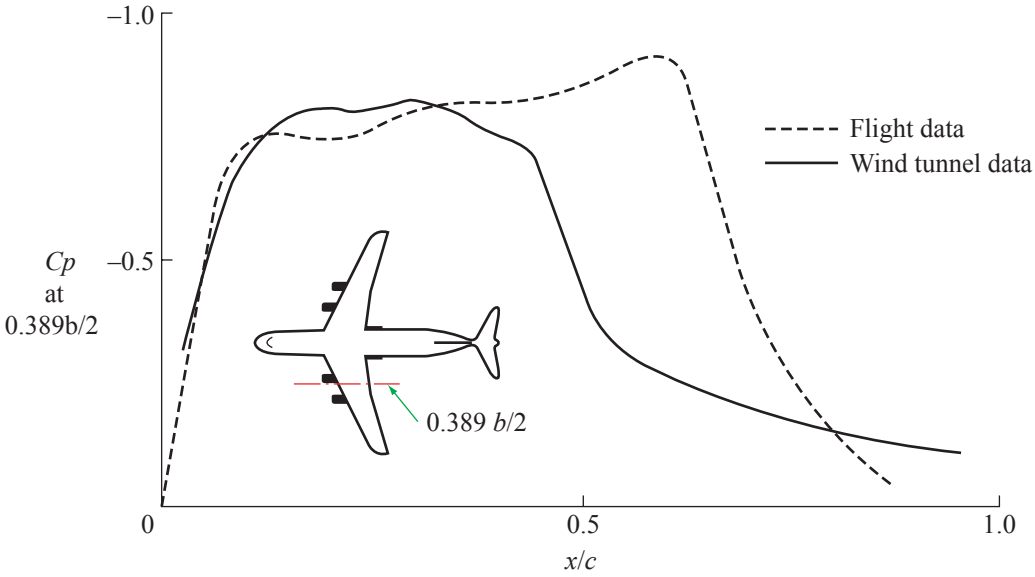

Sketch 6.8 Discrepancy in upper surface pressure distribution between wind-tunnel prediction and full-scale test (from Reference 48)

In a wind-tunnel test it is, therefore, important to ensure compatibility with the full-scale boundary layer at critical locations, *e.g.* the shock-wave position. Fixing transition at selected downstream locations ("aft fixing") is one example (there may be others) of a mean by which the boundary layer may be manipulated to produce a viscous flow behaviour closer to that forecast to occur at full-scale Reynolds numbers with natural transition located at a forward position. The turbulent boundary layer with aft fixing is thinner than that obtained with transition near the leading edge. Thus, downstream of transition, the viscous flow behaviour approximates to that expected at a higher Reynolds number. An important issue here is how to choose the simulation criterion that is used to associate this apparently increased Reynolds number with transition fixing position. This choice depends on the objectives of the particular test and it is prudent to compare results using more than one simulation criterion. A full account of use of the "aft-fixing" technique is currently in preparation and will be issued by ESDU. A detailed discussion is also given in reference 38.

7. DIRECT AND INDIRECT REYNOLDS NUMBER EFFECTS

Because it is possible that changes in Reynolds number may be accompanied by large changes in the surface pressure distribution, it is convenient to divide Reynolds number effects into two categories, *direct* and *indirect*, according to whether changes in Reynolds number are accompanied by significant changes in the external flow.

7.1 Direct Reynolds Number Effects

A direct Reynolds number effect is a change in the state of the viscous layer (*e.g.* boundary-layer transition location, boundary-layer thickness, the extent of a small local separation bubble *etc.*), which is caused primarily by Reynolds number change, in the presence of a given pressure distribution. In practice, Reynolds number changes always have a small influence on the external pressure distribution because of the change in boundary-layer displacement-thickness and, in turn, changes in the external pressure distribution influence boundary-layer development. However, these changes are small for a direct Reynolds number effect.

Thus, the boundary layer and external flows may be regarded as uncoupled, although a theoretical flow calculation technique may require an iterative procedure to deal with the relatively small interactions which may be present. An example of such a technique is given in Reference 49.

7.2 Indirect Reynolds Number Effects

Indirect Reynolds number effects are those in which the interaction between the boundary layer and external flow is strong. Typically this is so for the supercritical flow over a wing, where strong interaction between a shock wave and the boundary layer may cause significant separation, resulting in changes in both the external pressure distribution and, possibly, circulation. The relationship between direct and indirect Reynolds number effects is illustrated in Sketch 7.1.

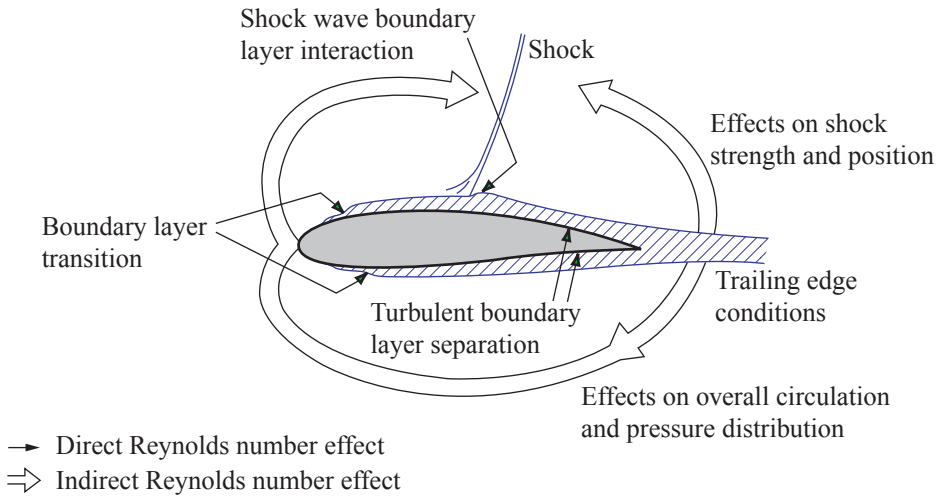

Sketch 7.1 Illustration of direct and indirect Reynolds number effects (from Reference 37)

8. PSEUDO REYNOLDS NUMBER EFFECTS

Matching flight Reynolds number in wind-tunnel tests, or making adequate corrections to tests at lower Reynolds numbers, is of great importance, particularly in situations when indirect Reynolds number effects may occur. Unfortunately, several phenomena associated with wind-tunnel testing may produce effects similar to those associated with a change in Reynolds number. It is therefore important to identify these pseudo Reynolds number effects and, where possible, to make suitable corrections for them. This is true both for wind-tunnel tests at full-scale Reynolds number, and, more significantly, for tests in lower Reynolds number facilities, the results of which are to be extrapolated to full-scale.

The possibility of the occurrence of pseudo Reynolds number effects is particularly high in transonic wind-tunnel testing, where the position of shock waves may be influenced significantly by small changes in test conditions. Additionally, where the tunnel walls are ventilated, by perforations or longitudinal slots (Sketch 8.1), the flow between the working section and plenum chamber interacts with the wall boundary layer.

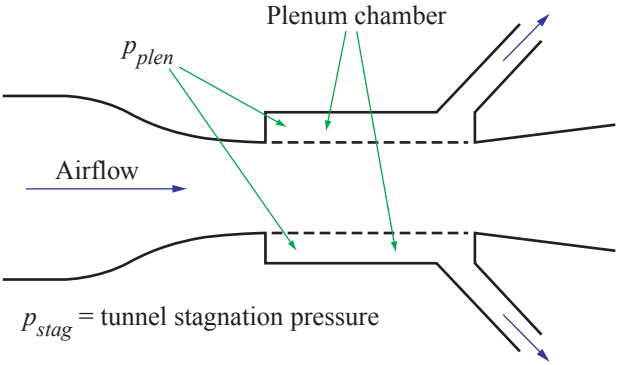

Sketch 8.1 Transonic wind tunnel with ventilated walls (schematic)

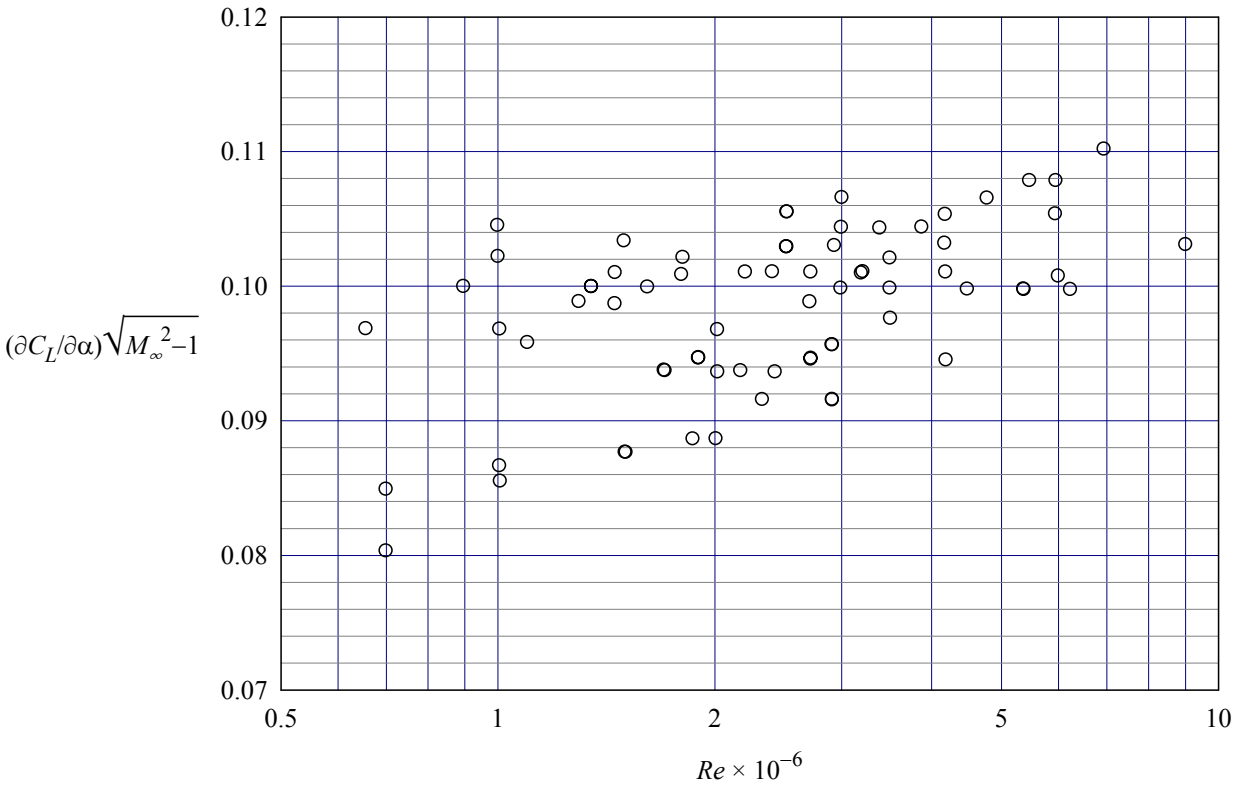

Sketch 8.2 Life-curve slope for NACA 0012 aerofoil for a variety of models in different facilities (from Reference 50)

Pseudo Reynolds number effects may be the cause of discrepancies between results obtained in different wind tunnels. This is illustrated in Sketch 8.2, which shows marked discrepancies in the lift-curve slope measured on the NACA 0012 aerofoil in several facilities. The tests were all made at a relatively low Mach number (≤ 0.55) and the lift-curve slope, in Sketch 8.2, has been factored to account for first order compressibility effects. The discrepancies are particularly marked at lower Reynolds numbers. From the results quoted, it is not clear to what extent the discrepancies are due to tunnel or model characteristics.

Pseudo Reynolds number effects are subdivided in Sections 8.1 to 8.3 into the three broad categories defined as Types I, II and III. These categories follow those given in Reference 51, with minor changes. This discussion is limited to the testing of static configurations such as wings, wing/body and wing/body/tail configurations. Pseudo Reynolds number effects are also associated with tests of moving configurations, such as propellers[51], which are not considered here.

8.1 Type I Effects

Parameters or corrections, required to reduce test data may, themselves, be influenced by a change in Reynolds number. Failure to account adequately for this dependency leads to Type I pseudo Reynolds number effects, which are particularly associated with tunnel calibration and wall interference effects.

8.1.1 Wind-tunnel calibration

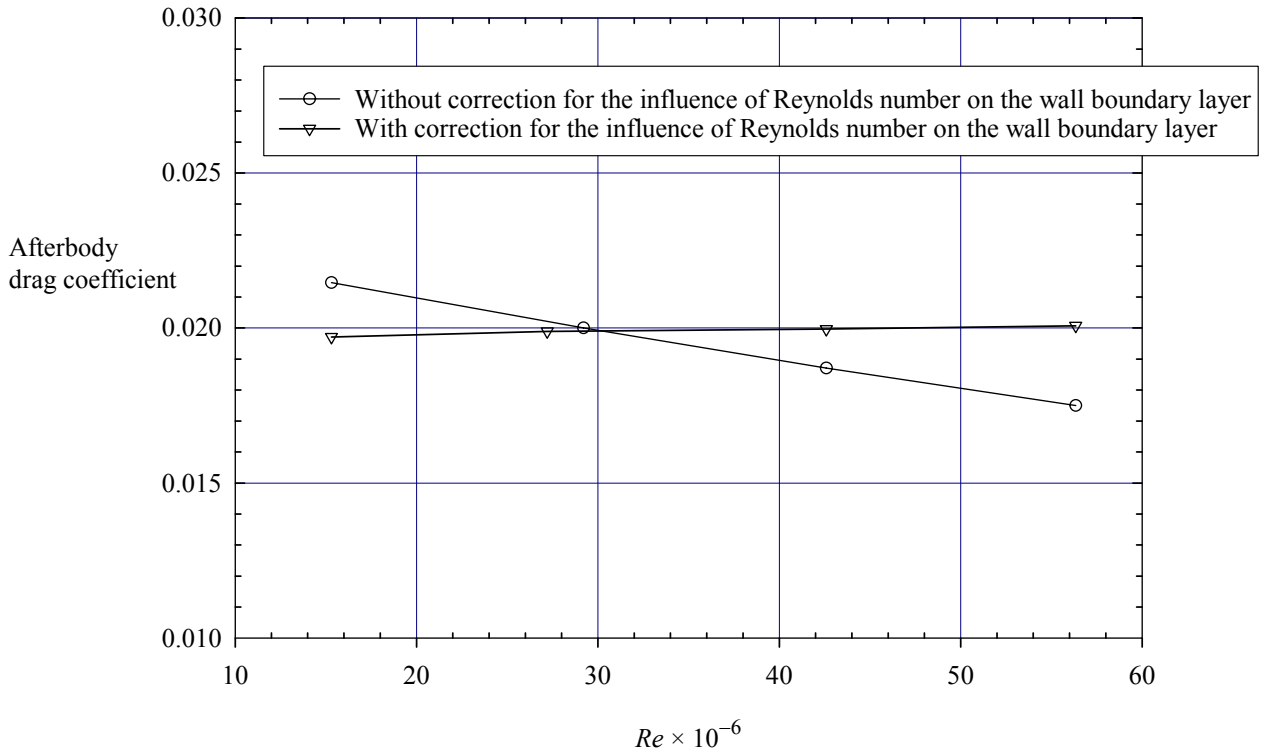

Sketch 8.3 Effect of wind-tunnel calibration on afterbody drag (from Reference 52)

Sketch 8.3 shows a reduction of drag coefficient with increasing Reynolds number in a set of uncorrected data. This may be mistaken for a genuine Reynolds number influence on drag, although the corrected data show that this is really a pseudo Reynolds number effect, caused by an uncorrected Reynolds number dependency in the calibration of the empty wind tunnel.

This dependency occurs because the thickness of the wall boundary layer depends on Reynolds number. For a ventilated wind-tunnel, the calibration which relates the working-section Mach number to the ratio of tunnel stagnation pressure, p_{stag}, and plenum-chamber pressure, p_{plen}, actually depends on the stagnation pressure used. This dependency is of particular significance in a pressurised tunnel and is most severe in wind tunnels with perforated, rather than slotted, walls.

Use of a simple calibration, at a single stagnation pressure and uncorrected for the Reynolds-number effects on the wall boundary layer, thus leads to an error, ΔM, in the calculated working section Mach number. A simple analysis, based on one-dimensional isentropic flow, shows that the error in drag resulting from this error in Mach number calibration is given by:

$$\Delta C_D = \frac{2S_t}{S_{ref}} \cdot \frac{\Delta M}{M_\infty(1 + 0.2M_\infty{}^2)} . \qquad (8.1)$$

This effect may be exacerbated if shock waves are present in the flow, because there may be significant changes in shock wave location and strength with Mach number. This may, for example, lead to significant errors in the prediction of the maximum lift coefficient on an aerofoil[53].

8.1.2 Wall interference

The importance of wall interference in transonic wind-tunnel testing is illustrated in Sketch 8.4 and Sketch 8.5. Sketch 8.4 shows a comparison between C_L *vs.* α measurements made on a generic wing-body-tail model in two perforated-wall tunnels of differing size (AEDC T1 and T4)[54]. Tests were made at 7% open area ratio in both tunnels and also at 3% in tunnel T1. In all tests the perforating holes were inclined at 60° to the freestream direction. The results obtained from the two tunnels agree closely for the 7% open area ratio but there was a significant change when the open area ratio was reduced to 3%. Although techniques are available to correct for wall interference for perforated walls[54], the results shown in Sketch 8.4 were obtained at high freestream Mach number ($M_\infty = 0.9$) with supercritical conditions ($M > 1$) in the region between the wing upper surface and the wall, which makes wall-effect correction particularly difficult. However, even at lower freestream Mach numbers, where the wall flow is subcritical, significant errors may be incurred if wall correction is ignored or dealt with inadeqately.

Investigations into the influence of the open area ratio, using both Euler and Navier Stokes codes[51], demonstrate the significance of the viscous terms in the effect of open area ratio and hence the potential for Reynolds number influence. Thus a change in Reynolds number may affect the influence of a perforated wall on, for example, the lift of a model and this may be interpreted erroneously as a genuine Reynolds number effect.

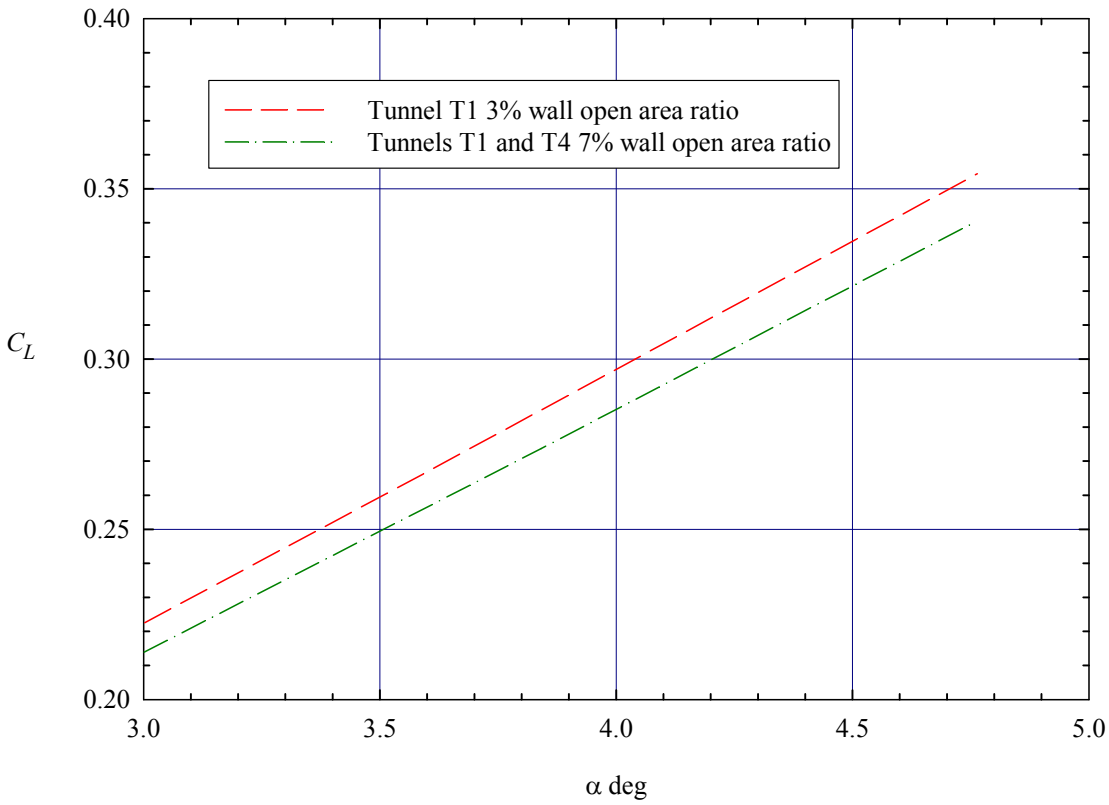

Sketch 8.4 Effect of porosity in perforated-wall tunnels (from Reference 54)

Blockage is the effective increase in the working-section airspeed due to the constraint imposed by the test-section boundaries (solid or ventilated walls, or constant pressure at the edge of an open jet). It is usually correlated in terms of blockage ratio (model frontal area divided by the cross-sectional area of the tunnel working section).

Sketch 8.5 shows the effect of blockage ratio on the pressure distribution measured on a wing using the same mounting system in the AEDC T16 tunnel (blockage ratio 0.16%) and the AEDC T4 tunnel (blockage ratio 2.6%). Both tests were made at a Reynolds number of 2.5×10^6. A large discrepancy is apparent, probably associated with an observed change in shock induced separation, which was accompanied by significant changes in shock wave strength and location on the wing.

This change in shock strength and location is qualitatively similar to that obtained by a change in Reynolds number. Where tests are conducted using, for example, different sized models in a given wind-tunnel, in order to cover a range of Reynolds numbers, a change in the characteristics of the shock wave, caused by a change in blockage, may be misinterpreted as a Reynolds number effect.

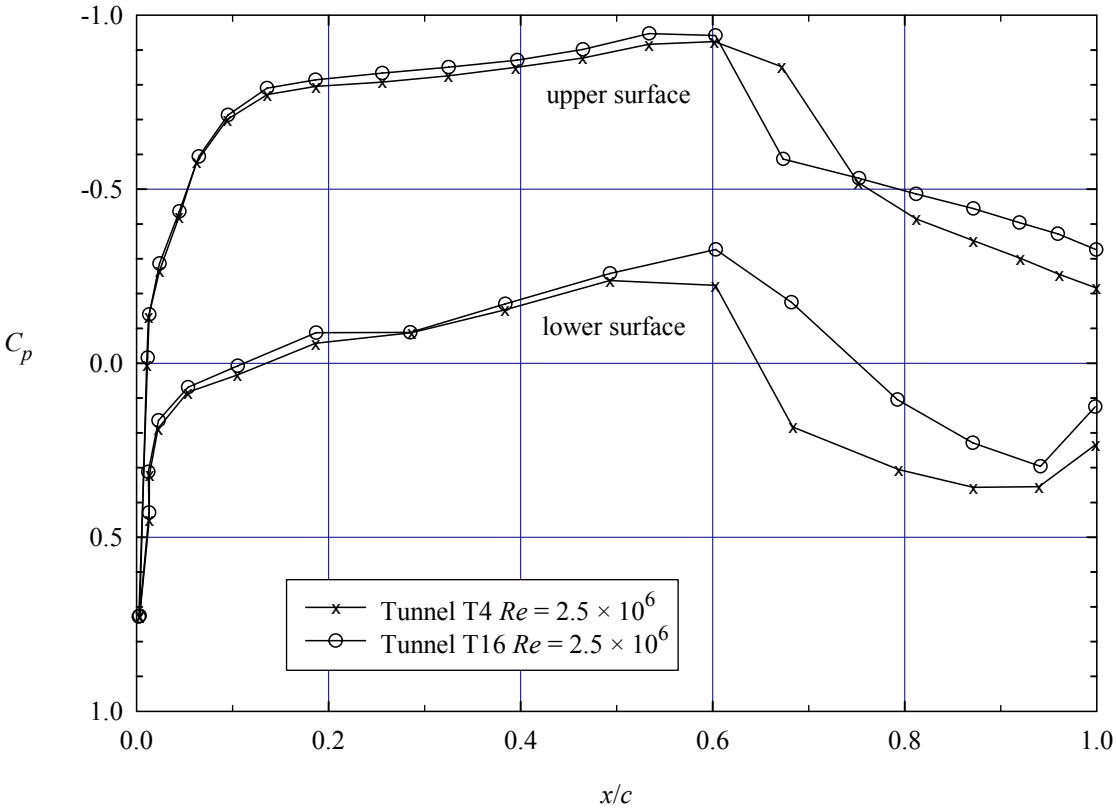

Sketch 8.5 Effect of blockage in perforated wall tunnels on wing models

The examples of Sketches 8.4 and 8.5 show that the effects of wall interference can be large. Where tests are made at different Reynolds numbers these may mask, or be mistaken for, genuine Reynolds-number effects unless suitable corrections are made.

Corrections for wall-interference effects in tunnels with solid walls are well established (*e.g.* Reference 55). However, in ventilated-wall tunnels, the solid-wall corrections must be modified by suitable factors. These factors are influenced by the geometrical properties of the tunnel, including those of the slotted or perforated wall, and are required to account for the flow between the working section and the tunnel plenum chamber. Because this flow is influenced by the thickness of the wall boundary layer, the factors are also influenced by the unit Reynolds number in the test section. It is believed[51] that failure to account for this effect could explain much of the apparent Reynolds number influence in Sketch 8.2.

Jacocks[56] correlated the effects of porosity with wall boundary-layer characteristics for a perforated wall with holes inclined at 60° and, using this correlation, a correction procedure has been developed for tunnels employing perforation holes inclined at this angle[54].

The above procedure assumes the "empty-tunnel" wall boundary layer is unchanged by the presence of the model. However, the flow field around the model influences the boundary-layer growth at the walls and this influence is, in general, Reynolds number dependent. This affects the local flow between the test section and the plenum chamber, introducing another Reynolds number dependent term into the wall correction procedure. Correction for this effect may be made by using a CFD method to estimate the effect of the model flow field on the wall boundary layer. When the flow about the model depends strongly on Reynolds number it is important to use an estimation method that takes account of the boundary layer, such as a Navier-Stokes code, since an Euler code may lead to a poor estimate of shock-wave position on the model.

Sidewall interference in tests on a two-dimensional aerofoil may also be important. For example, pressure gradients imposed by the aerofoil upper-surface pressure distribution may cause each side-wall boundary layer first to thin and subsequently to thicken, leading to the formation of two oblique shock waves, the effects of which may be felt at the aerofoil centre line. This is illustrated[57] in Sketch 8.6, where a disturbance in the form of a localised increase in the measured upper-surface pressure may be seen in a test with CAST 7 aerofoil. The estimated "interference free" comparison does not appear in Reference 57.

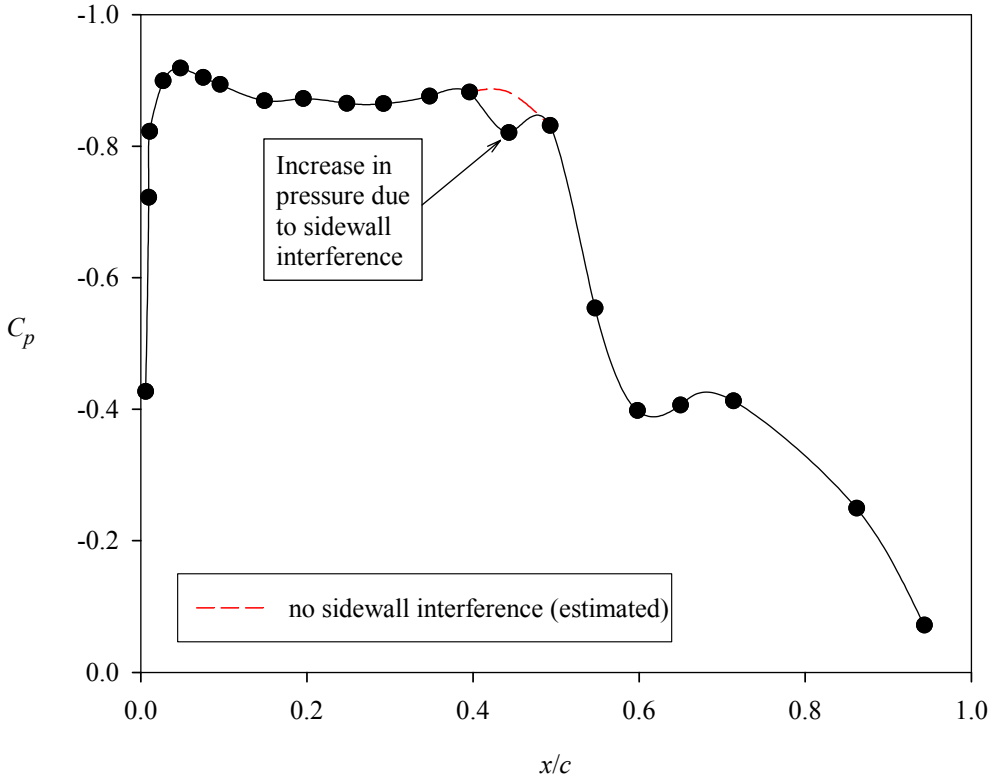

Sketch 8.6 Effect of sidewall interference on the centre-line pressure distribution of an aerofoil at $M_\infty = 0.790$ and $C_L = 0.560$ (from Reference 57)

A simple criterion may be applied to determine if the pressure distribution at the aerofoil centreline is likely to be affected by a side-wall generated shock wave. Such interference is likely to occur if:

$$b \leq \frac{2x_{shock}}{\sqrt{M_{shock}^2 - 1}}. \qquad (8.2)$$

For this criterion the shock wave is modelled as a Mach wave, originating on the tunnel side wall near the aerofoil leading-edge and propagating in a stream of Mach number M_{shock}. It is, therefore, only applicable for a weak side-wall shock wave where the Mach number over the upper surface of the aerofoil is approximately constant for much of the region upstream of x_{shock} (*i.e.* a "rooftop" pressure distribution).

8.2 Type II Effects

Systematic variations which are, or are thought to be, caused by changes in Reynolds number, may be wrongly attributed to a particular phenomenon if the involvement of other factors is not recognised. Instances of this include:

unrecognised Mach number effects,

confusion between the effects of transition location and extent, and boundary-layer growth,

misinterpretation of tunnel temperature effects.

Such misinterpretations may be of great significance when extrapolating wind-tunnel results to full scale and are known as Type II pseudo Reynolds number effects.

8.2.1 Unrecognised Mach number effects

It is often the case that, even at low freestream Mach numbers, local Mach numbers may be high. For example, local compressibility effects may be of significance on the elements of high-lift systems.

The importance of these local compressibility effects may be overlooked. For example, a change in Reynolds number, produced by altering the test stagnation pressure, may produce results which differ from those produced by a similar Reynolds number change effected by altering the temperature in a cryogenic tunnel. In the latter case, although the increase in freestream Mach number may appear to be insignificant, significant changes may occur in the locally transonic flow.

8.2.2 Transition location and extent

Sketch 5.16 shows that the transition location on a typical transport aircraft wing may differ between a wind-tunnel test and full scale flight and that the transition mechanisms, appropriate to the two cases, may also differ. The dependency of shock-wave/boundary-layer interactions on the local boundary-layer characteristics (Section 6) means that simply fixing the model transition location to coincide with full scale (*e.g.* by the use of surface roughness) may lead to inadequate modelling of the flow downstream of transition. Because the transition location and the development of the boundary layer downstream of transition are likely to differ between model and full scale, misinterpretations can occur both with free and, nominally, fixed transition.

Reference 51 describes a strategy to obtain data adequate for extrapolation to full-scale Reynolds numbers by conducting a series of transonic wind-tunnel tests either with free transition, at various stagnation pressures, or at constant stagnation pressure with transition fixed at a number of different locations. The interpretation of wind-tunnel tests with both fixed and free transition is therefore of importance.

The differing Reynolds number effects due to change in transition location and development of boundary layer thickness are illustrated in Sketch 8.7, which shows the lift curve slope, derived from wind-tunnel tests and corrected for wall interference, at $M_\infty = 0.3$ and $M_\infty = 0.7$, for a NACA 0012 aerofoil. At the lower Mach number the lift curve slope increases with increasing Reynolds number, consistent with boundary layer thinning as Reynolds number is increased. The tests at $M_\infty = 0.7$ were conducted at a

higher Reynolds number range and show the opposite trend, presumably because there is a significant forward movement of transition location, resulting in a thickening of the boundary layer at the trailing edge which outweighs what would otherwise be a thinning due to Reynolds number increase.

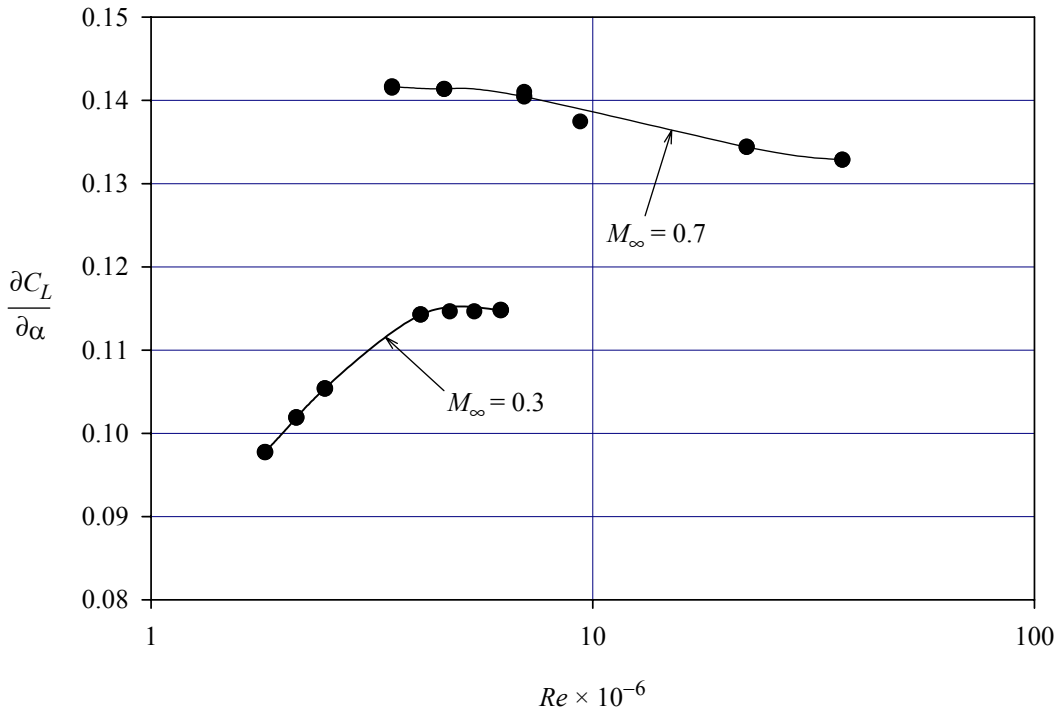

Sketch 8.7 Effects of transition location movement on a NACA 0012 aerofoil (from Reference 58)

Measurements on the surface of a cone[59] have shown a wide variation in the Reynolds number corresponding to free transition for different transonic wind tunnels. This variation was found to lie mainly in the range of $3 \times 10^6 \le Re \le 5 \times 10^6$, based on distance measured along the cone surface, although, in a few wind tunnels values as high as 10^7 were obtained. The variations are caused by differences in tunnel freestream flow characteristics and are discussed further in Section 8.3. Thus, particular care must be taken when comparing data acquired in different wind tunnels, because the transition locations may not be the same, even if the test Reynolds numbers are equal.

Another problem may arise when it is assumed that the extent of the transition region is small. Unless transition is forced, for example by a strong pressure gradient, this may not be the case (Section 5.1.1). When transition is not forced, a change in Reynolds number may also be accompanied by a change in the length of the transition region, which, in turn, influences the properties of the boundary layer downstream.

Where surface roughness bands are used to induce transition at a specific location, the roughness height must be chosen with care since, if too low, it will fail to produce transition, or may significantly increase the length of the transition region, and if it is too high, it will increase the local skin friction drag. The effect of surface roughness on transition is discussed in Section 5.1.4 and Equation (5.7) indicates that the required roughness for a particular application is sensitive to Reynolds number (and also Mach number). Thus, as test conditions are changed, the effects of over- or under-fixing may be mistaken for genuine Reynolds number effects.

8.2.3 Effect of temperature on unsteady phenomena

The effect of airstream temperature on local compressibility effects at low freestream Mach number is referred to in Section 8.2.1. A further problem may arise, for example, on tests involving unsteady aerodynamic phenomena, such as buffet.

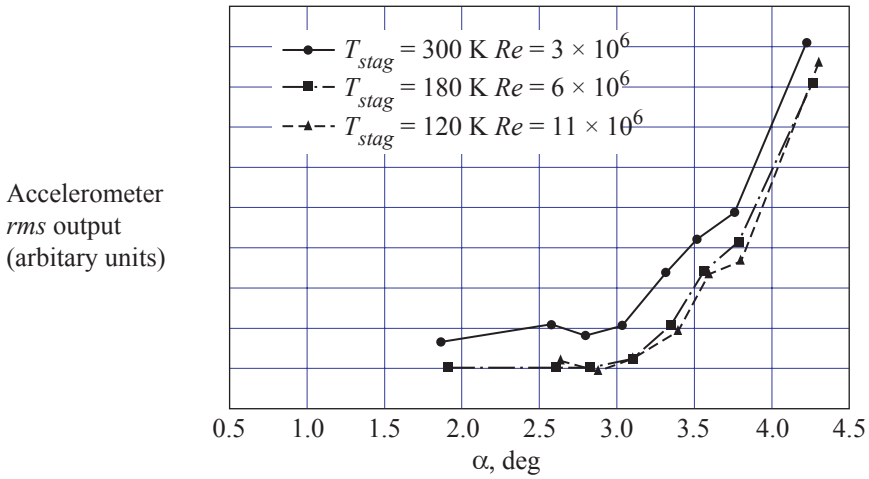

(a) Output from accelerometer at mid-span

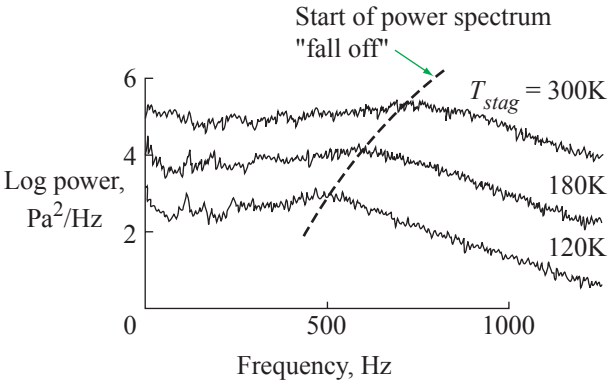

(b) Pressure power spectra

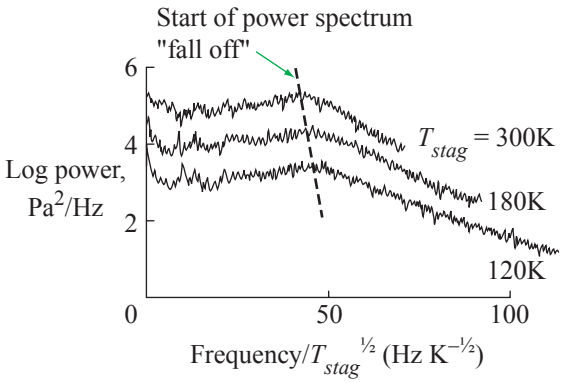

(c) Power spectra, as in (b), divided by $\sqrt{T_{stag}}$

Sketch 8.8 Effect of temperature on measured accelerometer and pressure fluctuations (from Reference 51)

This is illustrated in Sketch 8.8 which shows the output of an accelerometer, mounted at mid span on a half model of a transport aircraft, which was tested at a number of Reynolds numbers and stagnation pressures[51]. Sketch 8.8(a) shows that, although there is a rapid increase in the accelerometer *rms* output above $\alpha \approx 3$ deg in all tests, this output is generally higher at the lowest Reynolds number. This correlates with pressure measurements, taken directly on the wing surface (Sketch 8.8(b)), where the power spectrum starts to fall off at a higher frequency at the lower Reynolds numbers. Sketch 8.8(c) shows that, when the frequency is divided by $\sqrt{T_{stag}}$, the pressure power spectrum commenced to fall off at nearly the same point in all three tests. This indicates that the fall off may be influenced by a non-dimensional parameter, similar to a Strouhal

number, equal to the flow disturbance wavelength multiplied by its frequency and divided by the speed of sound. Although further details of these tests are not given in Reference 51, they indicate that it may be erroneous to attribute the effect shown in Sketch 8.8(a) to Reynolds number influence alone.

8.3 Type III Effects

Type III pseudo Reynolds number effects are caused by factors, other than Type I effects (Section 8.1), which lead to significant differences between conditions in the wind tunnel and in free flight. Such factors include:

noise and freestream turbulence,

humidity,

heat transfer effects,

model surface quality and model flexibility,

model support effects.

8.3.1 Noise and freestream turbulence

Reference 37 indicates that the effects of freestream noise and turbulence on transition location (discussed in Section 5.1.3) are difficult to distingush. However, thresholds may be set for both noise and turbulence, below which there is little influence on the flow. In Section 5.1.3 it is established that for freestream non-dimensional turbulence intensity the threshold is $T_\delta \approx 0.001$. For noise[48], this threshold corresponds to an *rms* variation in the pressure coefficient on a cone (with a semi-apex angle of 5 deg) of approximately 1% of the mean value. This conclusion is based on tests on the cone in a large number of transonic tunnels[59].

Freestream noise and turbulence are both influenced by wind-tunnel unit Reynolds number (Reynolds number per metre), rather than the Reynolds number based on the model characteristic length and this may lead to associated pseudo Reynolds number effects.

Pseudo Reynolds number effects, caused by freestream noise and turbulence, may be of particular significance when comparing tests made in different wind tunnels in which freestream noise and turbulence levels differ substantially. This is illustrated in Sketch 8.9 which shows the variation of minimum drag coefficient, C_{Dmin}, with Reynolds number measured, in two tunnels, on a $1/9^{th}$ scale aircraft model. In both cases free transition was allowed.

A significant kink is apparent in each curve, although this appears at a lower Reynolds number in the Calspan 8 TWT test than in the Ames 11 TWT test. This may have been caused by differing levels of freestream turbulence in the two wind tunnels, the Calspan 8 TWT having the higher turbulence level. This view is supported by measurement of the natural transition position on the surface of a cone[59], which, indeed, indicated a higher turbulence level in this wind tunnel.

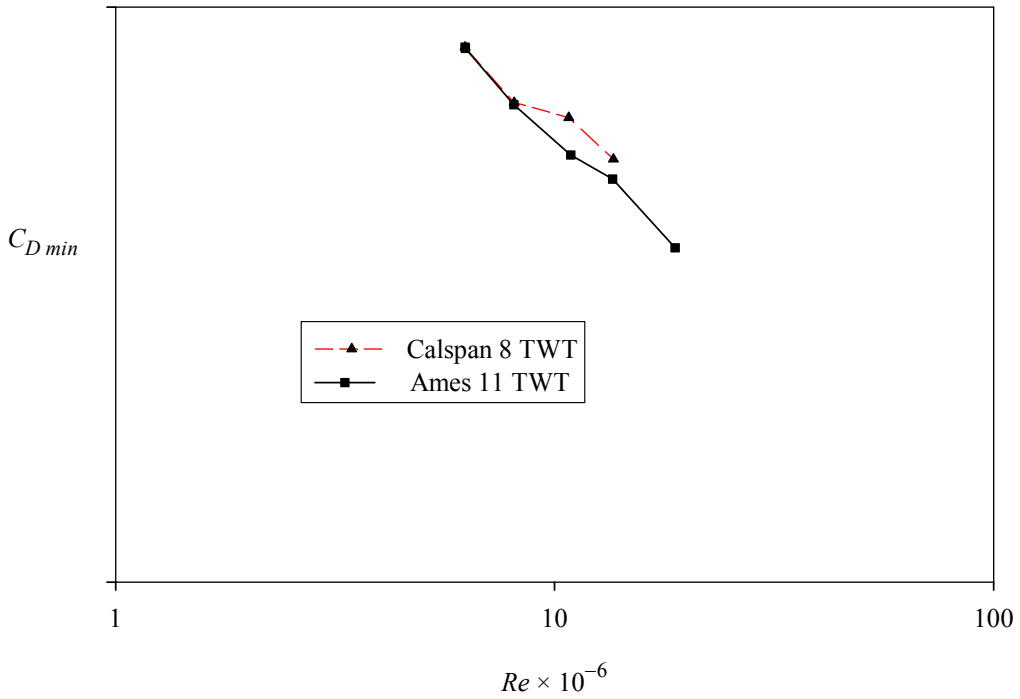

Sketch 8.9 Minimum drag coefficient for YF-16 aircraft model, measured in two different tunnels at $M_\infty = 0.9$ (derived from Reference 60)

As well as affecting transition, freestream turbulence may also influence boundary layer development[61] and separation. An example of this is shown in Sketch 8.10. Tests made at the same Reynolds number in the two wind tunnels show differences in the region where the onset of separation is affecting the lift curve. Because of the lower Reynolds number it would be expected that the separation causing the change in lift curve slope would occur at a lower incidence in the Calspan 8 TWT test. The fact that the opposite occurred is due to the higher freestream turbulence in that tunnel.

Symbol	Test	Reynolds number per metre	Tunnel
○	A	0.914×10^6	(Ames 11 - TWT)
●	B	2.13×10^6	(Ames 11 - TWT)
☆	C	0.914×10^6	(Calspan 8 - TWT)

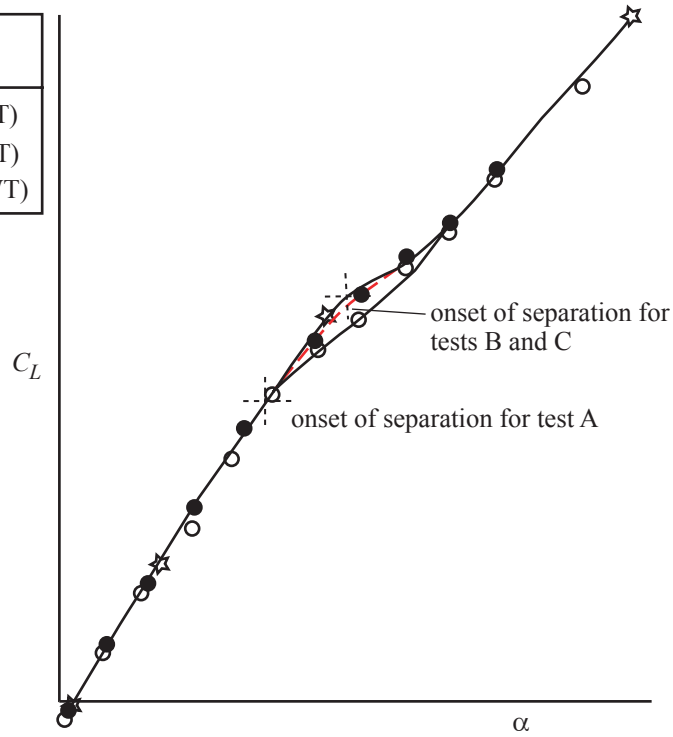

Sketch 8.10 Variation of C_L with α for a YF-16 aircraft model, measured in two different tunnels at $M_\infty = 0.9$ (derived from Reference 60)

8.3.2 Heat transfer effects

Heat transfer, either from the flow to the model or *vice versa* may influence the boundary layer significantly. This is particularly significant in wind tunnels having a short run time, such as blow-down tunnels. This was shown by tests in a cryogenic tunnel[62], in which an OALT25 aerofoil was tested at $M_\infty = 0.7$ with a tunnel stagnation temperature of 220K, an incidence of 0.25 deg and a Reynolds number of 7.5×10^6. Shortly after the test was commenced, the ratio of the actual wall temperature to the equilibrium wall temperature was 1.25 and, under these conditions, transition was found to be at 0.38*c*. As the run progressed and the wall temperature neared the equilibrium value, the transition position moved to 0.53*c*. These results were in agreement with calculations using the e^N method (Section 5.1.1), including non-equilibrium model temperature effects, and assuming a value of $N = 7$. Separate tests, in equilibrium conditions, showed that an increase in Reynolds number to approximately 11×10^6 would be required to bring the transition point forward from 0.53*c* to 0.38*c*. Thus, if the model is at a temperature higher than the equilibrium value, early transition occurs, corresponding to an apparently higher Reynolds number.

Tests to determine the position on a cone having a semi-apex angle of 5 deg[63], over a much more limited range of temperature ratios (0.95 to 1.08) indicated that, over this range, the effective Reynolds number could be estimated using:

$$\frac{Re_{eff}}{Re_{eq}} = \left(\frac{T_w}{T_{eq}}\right)^{-7}. \qquad (8.3)$$

This was found to apply over the whole range of Mach numbers of the test, namely 0.55 to 2.0.

8.3.3 Humidity

Humidity in an airstream may affect a flow in two ways:

Properties of the air such as γ and R may be changed by the presence of *water vapour*. In Section 3.3 it is shown that only γ is significant in achieving dynamic similarity.

Significant energy interchange may be caused by the *condensation* and *evaporation* of the water vapour at various locations in the flow field.

The variation in properties is small. In Reference 65 it is shown that, for saturated air, at Standard sea level temperature and pressure, the value of R is increased by 0.8% over its dry air value, while γ is reduced by 0.2%, compared to the dry air values.

Sketch 8.11 shows the effects of humidity calculated using an Euler code including a semi-empirical allowance for condensation effects[64]. Very significant changes are found, both in the surface pressure distributions and in the force and moment coefficients, obtained by integrating the pressure distributions. Changes in R and γ from the dry air values (estimated using the methods of Reference 65) and corresponding to the stated humidity levels used in the simulation were 0.2% and –0.04% respectively. It thus seems likely that the effects are due to the evaporation and condensation of water vapour as the flow passes over the aerofoil. This was confirmed[65] by a simple calculation in which the observed increase in local pressure, at approximately 0.2c (Sketch 8.11(a))*, was modelled by a discrete condensation shock. Sketch 8.12 shows good agreement between this simple calculation and the local pressure coefficient derived from Sketch 8.11(a). The convergence of the upper surface pressure distributions further downstream indicates a subsequent vaporisation of the condensate.

When there is a likelihood of significant condensation effects, the air in a wind tunnel is dried so as to reduce the water vapour content to a level where significant energy exchange cannot occur if condensation takes place.

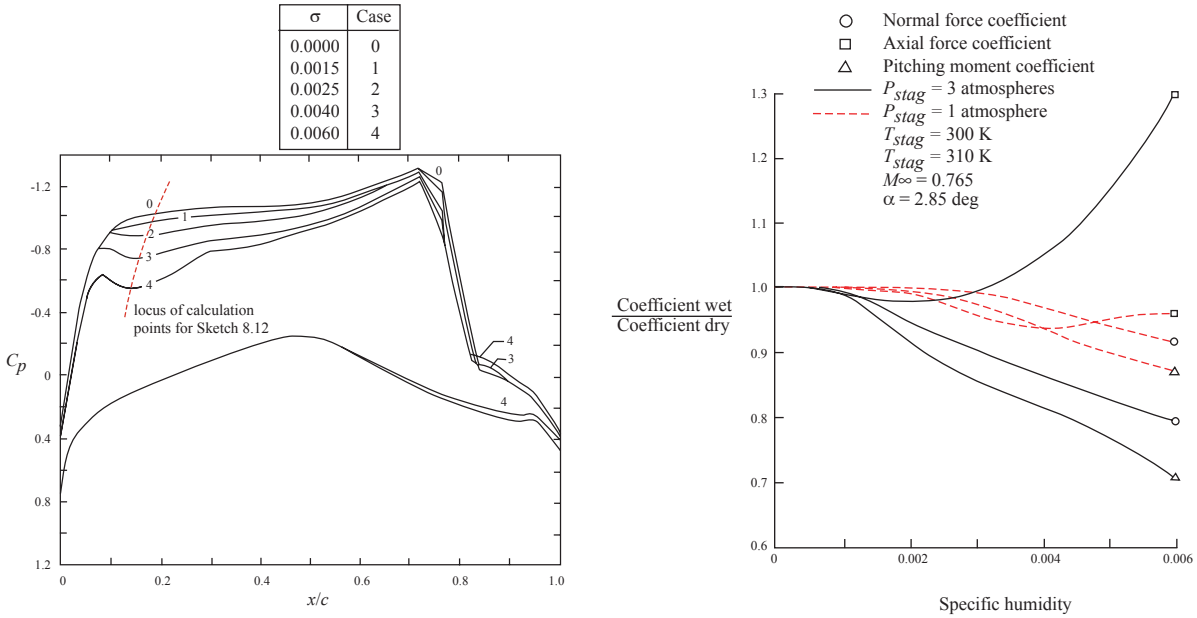

(a) Pressure coefficients (p_{stag} = 3 atm.) **(b) Force and moment coefficients**

Sketch 8.11 Calculated effect of condensation at different specific humidity levels on a CAST 10 aerofoil (from Reference 64)

* Calculations were made at the local pressure coefficient maxima for cases 4 to 2 (Sketch 8.11(a)). The locus of these maxima was extrapolated to obtain calculation points for cases 1 and 0.

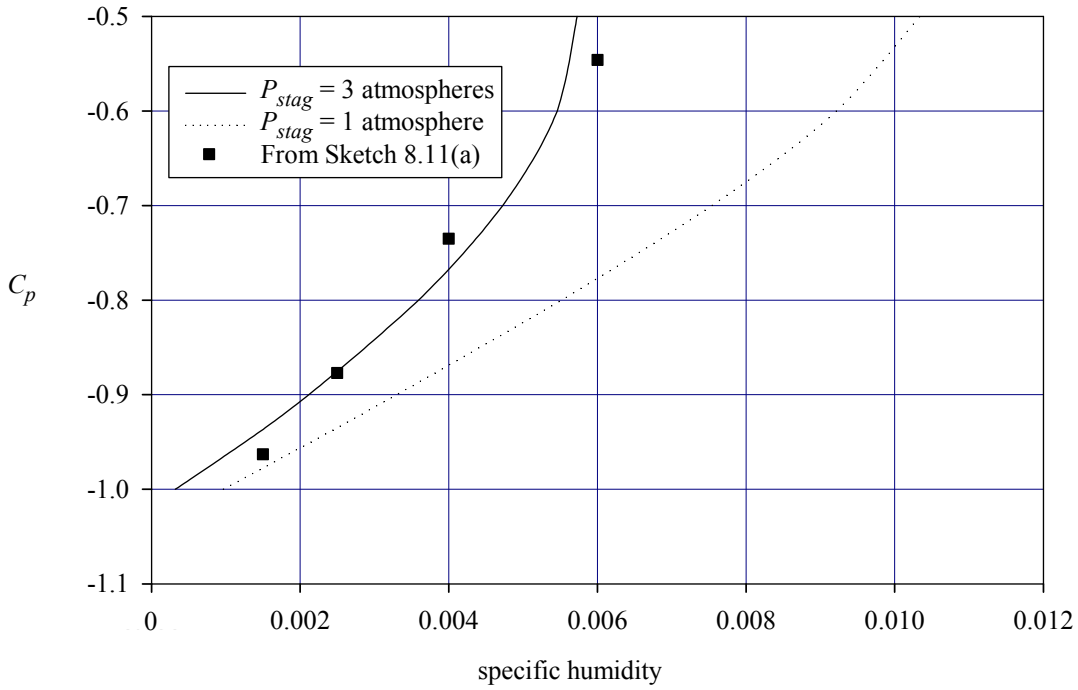

Sketch 8.12 Estimation of condensation effect on local pressure at approximately 0.2c using discrete condensation shock (from Reference 65)

8.3.4 Model accuracy, surface quality and flexibility

In Reference 66 a description is given of the effect of profile tolerance on the performance of a supercritical aerofoil (Lockheed CRYO 12X). A 152mm (6 inch) chord model was made and its surface profile measured. Deviation from the design profile is shown in Sketch 8.13(a). The surface pressure distribution on the aerofoil was calculated, using a coupled viscous/inviscid method. The calculation was repeated for two other profiles, with improved tolerance, derived by scaling the errors in the original model. It can be seen that the effect of tolerance was very pronounced, the greater tolerances leading to the formation of a significant shock wave (Sketch 8.13(b)). This illustrates the potential danger of investigating Reynolds number effects by the use of models of different scale in the same wind tunnel without careful attention being paid to allowable model profile tolerance.

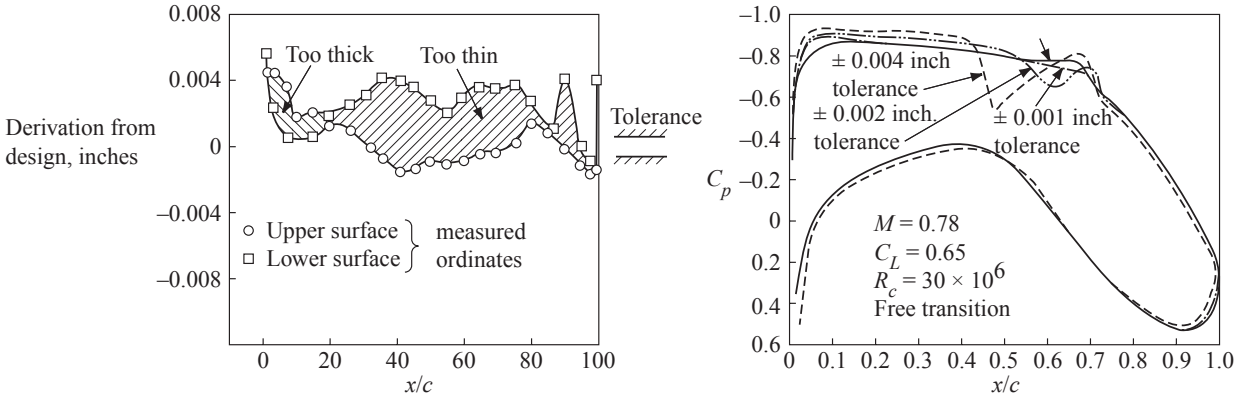

(a) Profile error **(b) Pressure distribution**

Sketch 8.13 Accuracy of aerofoil profile and effect on pressure distribution (from Reference 66)

In addition to the problems caused by inadequate tolerance in the basic profile, the presence of surface roughness may:

cause premature transition, and/or

increase the skin friction and rate of growth of a turbulent boundary layer.

Either may be mistaken for genuine Reynolds number effects.

The effect of roughness on transition is described in Section 5.1.4. The degree of surface roughness that just influences free transition is Reynolds number dependent and therefore any roughness above this level may further confuse the interpretation of the Type II pseudo Reynolds number effects described in Section 8.2.2.

An increase in skin friction occurs, for a turbulent boundary layer, when the roughness height exceeds that of the viscous sublayer. Experiments by Nikuradse[67] showed that, for fully developed turbulent flow in a pipe of circular cross-section, this occurs when

$$\frac{e}{\nu}\sqrt{\frac{\tau_w}{\rho}} > 5\,, \tag{8.4}$$

which implies the need for very smooth surface finish for tests at high Reynolds number, for which τ_w is likely to be large. This is illustrated in Sketch 8.14 (from Reference 69) where calculations using VGK[49] were made, together with Equation (8.4), to evaluate the limiting value of e/c at different Reynolds numbers for an OAT15A aerofoil at $M_\infty = 0.75$, $C_L = 0.6$, with transition at $0.05c$.

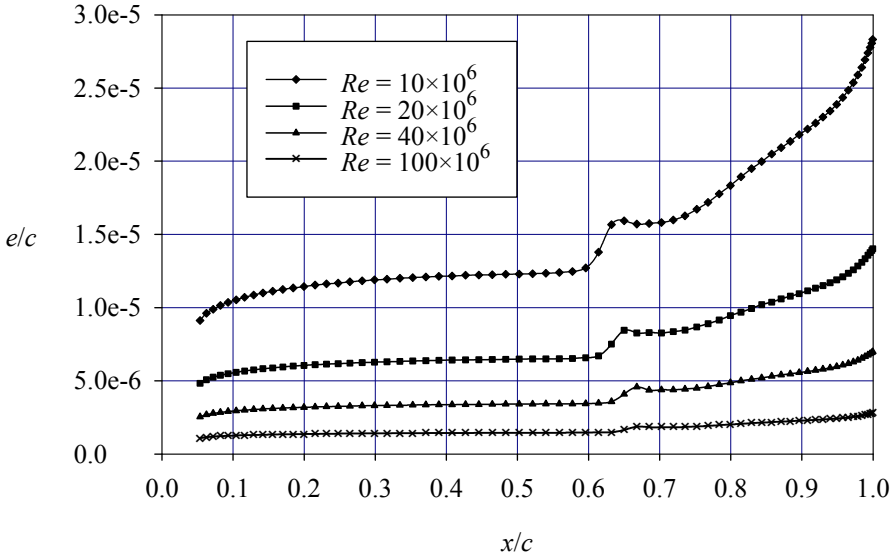

Sketch 8.14 Limiting roughness height for the upper surface of OAT15A aerofoil (M_∞ = 0.75, C_L = 0.6, transition at 0.05c) (from Reference 69)

8.3.5 Model support effects

Wind-tunnel model mounting systems produce interference which influences drag and other parameters. Corrections[55] may be applied to minimise this interference but the physical size of the support system may well require some modification to the geometry of the model. For example, the rear fuselage geometry may require alteration to accommodate a tail sting. The effect of Reynolds number changes may differ between the modified and the desired geometry. It may also be the case that the particular support geometry employed may give rise to Reynolds number effects which would not generally be included in the correction procedure used.

Earnshaw *et al*.[68] drew attention to a problem that may arise with half-models mounted on the wind-tunnel wall or floor. Tests were made, at low speed (M_∞ = 0.2) and Reynolds numbers of 5.0 × 10^6 and 6.45 × 10^6, on a floor-mounted wing-fuselage half-model of a large transport aircraft. At the lower Reynolds number, there was a sharp nose-down break in the pitching moment curve at the stall, although tests at the higher Reynolds number, and on a full-span model, showed a mild nose-up break. It was found that the stalling behaviour at the lower Reynolds number could be made to conform to the other cases by re-energising the floor boundary layer, by the use of blowing upstream of the model, or by using a plinth to bring the model just clear of the floor boundary layer. However, the behaviour was highly dependent on the plinth height. It was concluded that the effect was due to changes in the downwash distribution over the wing, which was sensitive to the floor boundary layer and therefore exhibited pseudo Reynolds-number effects.

9. CONCLUDING REMARKS

In order for dynamic similarity to exist between a wind-tunnel test and the full-scale flow, M_∞, Re and γ should be equal in the two cases, the assumptions implicit in the use of the Navier-Stokes equations should be applicable in each case and there should be no significant heat transfer between the external flow and the solid surface, either for the model or the full-scale flow. It is also necessary to reproduce boundary conditions exactly, although this is not strictly possible because of the presence of such factors as the wind-tunnel walls, the model support system and freestream turbulence.

Since γ depends only on the number of atoms which constitute a gas molecule, a close match to air may be obtained by testing in any diatomic gas, such as nitrogen. The use of nitrogen may be desirable if tunnel Reynolds number is to be increased by using a cryogenic wind tunnel, in which a reduced stagnation temperature is used in order to increase density and decrease viscosity.

In many cases it is not possible, in a wind-tunnel test, to match full-scale Reynolds number and Mach number. In the case of a flow where compressibility has a significant influence (particularly one in which shock waves are present) it is essential to match Mach number and a mismatch in Reynolds number must therefore be tolerated. The main effects of a mismatch in Reynolds-number are changes in the boundary-layer development and transition location and in flow separation characteristics.

There are many potential causes of boundary-layer transition and many influencing factors. For most transport aircraft, transition locations on the wing are close to the leading edge. This may not be the case for a test conducted at a lower Reynolds number and roughness strips may be required in order to induce transition at the required locations on the upper and lower surfaces.

Where shock-induced separation is likely, the boundary-layer state at the shock location is of prime importance. Since fixing the position of the roughness strip to achieve the correct transition location will not ensure compatibility of the model and full-scale boundary layers at the shock wave, a more complex strategy is required in order to extrapolate the wind-tunnel results to full scale correctly. This involves testing over a range of Reynolds numbers, where this can be achieved at constant Mach number in a given tunnel, or, if this is not possible, testing over a range of transition strip locations[38].

In order to interpret a wind-tunnel test in a satisfactory manner, accurate knowledge of the freestream Mach number, the Reynolds number and the transition location are required. For the latter, guidance may be obtained from flow visualisation techniques[45].

Because exact dynamic similarity cannot be achieved in a wind-tunnel test, a number of phenomena may be present, which influence results in a manner similar to a change in test Reynolds number. It is necessary to be aware of these, so called, pseudo Reynolds-number effects in wind-tunnel testing and, where possible, to apply suitable corrections to reduce their influence.

10. REFERENCES

1. ANDERSON, J.D. — *Fundamentals of aerodynamics*. McGraw-Hill Education (ISE Editions), ISBN 0-07-118146-6, 2001.
2. HOUGHTON, E.L. CARPENTER, P.W. — *Aerodynamics for engineering students*. Butterworth-Heinemann, ISBN 0-34-054847-9, 1993.
3. U.S. Standard Atmosphere, 1976. U.S. Government Printing Office, Washington, D.C., 1976.
4. ARIS, R. — *Vectors, tensors and the basic equations of fluid mechanics*. Dover Books on Engineering, ISBN 0-486-66110-5, 1990.
5. ESDU — Properties of a standard atmosphere. Data Item number 77021, ESDU, October 1977.
6. LIEPMANN, H.W. ROSHKO, A. — *Elements of gasdynamics*. Dover Publications, ISBN 0-48-641963-0, 2002.

7.	YOUNG, A.D.	*Boundary Layers*. BSP Professional Books, ISBN 0-632-02122-5, 1989.
8.	OBREMSKI, H.T. MORKOVIN, M.V. LANDAHL, M.T.	A portfolio of stability characteristics of incompressible boundary layers. AGARDograph 134, 1969.
9.	MICHEL, R.	Etude de la transition de les profiles d'aile; etablissement d'un'critére de determination de point de transition en calcul de la trainee de profil incompressible. ONERA, Tech. Report 1/1578A, 1951.
10.	VAN INGEN, J.L.	A suggested semi-empirical method for the calculation of the boundary layer transition region. VTH 74, Dept. of Aero. Eng., Tech. Univ., Delft, 1956.
11.	SMITH, A.M.O. GAMBERONI, N.	Transition pressure gradient and stability theory. Proc. Int. Congr. App. Mech., 9, 4, p. 234, 1956.
12.	GRANVILLE, P.S.	The calculation of the viscous drag of bodies of revolution. David W. Taylor Model Basin, Rep. 849, 1954.
13.	JOSLIN, R. D.	Overview of laminar flow control. NASA TP-1998-20705, 1998.
14.	GOLDSTEIN, M.E.	The evolution of Tollmien-Schlichting waves near a leading edge. Journal of Fluid Mechanics, Vol. 127, pp. 59-81, 1983.
15.	GOLDSTEIN, M.E.	Scattering of acoustic waves into Tollmien-Schlichting waves by small streamwise variations in surface geometry. Journal of Fluid Mechanics, Vol. 154, pp. 509-529, 1985.
16.	GOLDSTEIN, M.E. LEIB, S.J. COWLEY, S.J.	Generation of Tollmien-Schlichting waves on interactive marginally separated flows. Journal of Fluid Mechanics, Vol. 181, pp. 485-517, 1987.
17.	BERTOLOTTI, F.P. CROUCH, J.D.	Simulation of boundary layer receptivity to spike stage. NASA CR-191413, 1992.
18.	WIEGEL, M. WLEZIEN, R.W.	Acoustic receptivity of laminar boundary layers over wavy walls. AIAA-93-3289, 1993.
19.	CROUCH, J.D.	Theoretical studies on the receptivity of boundary layers. AIAA 94-2224, 1994.
20.	DRYDEN, H.L.	Transition from laminar to turbulent flow. In, Turbulent flows and heat transfer (ed. C.C. Lin). Princeton University Press, N.J., 1959.
21.	MACK, L.M.	Boundary layer stability theory. JPL, Pasedena, California, Report 900-277, 1969.
22.	SCHILLER, L.	Handbuch der Exp. Physik. Leipzig, IV, 4, p. 189, 1932.
23.	BRASLOW, A.L.	Review of the effect of distributed surface roughness on boundary layer transition. AGARD Rep. 254, 1960.
24.	SMITH, A.M.O. CLUTTER, D.W.	The smallest height of roughness capable of affecting boundary layer transition. Jour. of Aerospace Sciences, April 1959.

25.	VAN DRIEST, E.R. BLUMER, C.B.	Effects of roughness on transition in supersonic flow. AGARD Rep. 255, 1960.
26.	GÖRTLER, H.	Über ein dreidimensionale Instabilität laminarer Grenzschichten an konkaven Wänden. Math. Phys. Klasse, 2, pp. 1-16, 1940. On the three-dimensional instability of laminar boundary layers on concave walls. NACA TM-1375, 1954 (Translation).
27.	LIEPMANN, H.W.	Investigation of boundary layer transition on concave walls. NACA Wartime rep. W-87, 1945.
28.	ANSCOMBE, A. ILLINGWORTH, L.N.	Wind tunnel observations of boundary layer transition on a wing at various angles of sweepback. ARC, R&M 2968, 1956.
29.	STRATFORD, B.S.	Flow in the laminar layer near separation. ARC, R&M 3002, 1954.
30.	ARNAL, D. HABIBALLAH, M. COUSTOLS, E.	Laminar instability theory and transition criteria in two- and three-dimensional flow. La Recherche Aerospatiale, No. 2, 1984.
31.	WHITE, E.B. SARIC, W.S. GLADDEN, R.D. GABET, P.M.	Stages of swept wing transition. AIAA paper 2001-0271, 39th Aerospace Sciences Meeting and Exhibition, 2001.
32.	MALIK, M.R. Li, F. CHOUDHARI, M. M. CHANG, C.L.	Secondary instability of crossflow vortices and swept-wing boundary layer transition, Journal of Fluid Mechanics. Vol. 339, 1999.
33.	HAYNES, T.S. REED, H.L.	Simulation of swept-wing vortices using non-linear parabolized stability equations. Journal of Fluid Mechanics, Vol. 405, 2000.
34.	PFENNIGER, W.	Flow problems of swept low-drag suction wings of practical construction at high *Re*. Annals of NY Acad. of Sci., Vol. 154, Art. 2 pp. 672-703, 1968.
35.	DEYHLE, H. BIPPES, H.	Disturbance growth in an unstable three-dimensional boundary layer and its dependence on initial conditions. J. Fluid Mechanics, Vol. 316, 1996.
36.	CROUCH, J.D. NG, L.L.	Variable N-factor method for transition prediction in three-dimensional boundary layers. AIAA Journal, Volume 38, No. 2, pp. 211-216, 2000.
37.	ELSENAAR, A. BINION, T.W. Jr. STANEWSKY, E.	Reynolds number effects in transonic flow. AGARDograph No. 303 (AGARD-AG-303), 1988.
38.	ELSENAAR, A. HAINES, A.B.	Shock-wave boundary-layer interactions. AGARD Advisory Report No. 224 (AGARD-AR-224), 1988, p. 96.
39.	HEFER, G.	ETW- A facility for high Reynolds number testing. IUTAM Symposium Transsonicum IV, Göttingen, Germany, 2002.

40. WONG, P.W.C. MAINA, M. — Studies of methods and philosophies for designing hybrid laminar flow wings. ICAS Proceedings, ICAS 2000-2.8.2., Harrogate, U.K., August 2000.

41. CURLE, N. SKAN, S.W. — Approximate methods for predicting separation properties of laminar boundary layers. Aero. Quaterly, 8, p. 257, 1957.

42. ESDU — A method of estimating a separation boundary for two-dimensional aerofoil sections in transonic flow. ESDU Data Item 81020, December 1981.

43. ESDU — VGK method for two-dimensional aerofoil sections. Part 3: Estimation of a separation boundary in transonic flow. ESDU Data Item 97030, October 1997.

44. HAMMA, W. — Neu entwickelte Träflugelprofile für $Re<10^5$ mit den zugehörigen Polaren und Ergebnissen aus Grenzschichtbeobachtungen an diesen Profilen. Diploma thesis (Teil II), Institut für Aerodynamik und Gasdynamik, Technische Hochscule, Stuttgart, 1963.

45. HOLT, D.R. CHISHOLM, I. — Surface flow visualisation in aircraft design. ESDU Data Item 03014, March 2004.

46. DELERY, J. MARVIN, J.G. — Shock-wave boundary-layer interactions. AGARDograph No. 280 (AGARD-AG-280), 1986.

47. PEARCEY, H.H. — Some effects of shock-induced separation of turbulent boundary-layer in transonic flow past aerofoils. ARC R&M 3108, 1959.

48. LOVING, D. L. — Wind-tunnel-flight correlation of shock-induced separated flow. NASA-TN-D-3580, 1966.

49. ESDU — VGK method for two-dimensional aerofoil sections Part 1: Principles and Results. ESDU Data Item 96028, April 2004.

50. AGARD — Wall interference in wind tunnels. Fluid dynamics. AGARD-CP-335, 1982.

51. HAINES, A.B. YOUNG, A.D. — Scale effects on aircraft and weapon aerodynamics. AGARDograph 323, (AGARD-AG-323), 1994.

52. KENNEDY, T.L. — An evaluation of wind tunnel test techniques for aircraft nozzle afterbody testing at transonic Mach numbers. AEDC-TR-80-8, (AD-A091775), 1980.

53. AULEHLA, F. — Calibration-related pseudo-Reynolds number trends in transonic wind tunnels. Journal of Aircraft, Vol. 29, 1992, pp. 545-552.

54. SICKLES, W. ERICKSON, J. — Wall interference correction for three-dimensional transonic flows. AIAA 90-1408, 1990.

55. POPE A. GOIN, K. — High speed wind tunnel testing. Krieger, 1978.

56. JACOCKS, J.L. — Aerodynamic characteristics of perforated walls for transonic tunnels. AEDC-TR-77-61 (AD0409040), 1977.

57. ASHILL, P.R. — Effects of sidewall boundary layers on aerofoils mounted from sidewalls of wind tunnels – experimental evidence and developments of theory. Royal Aircraft Establishment, TR 83065, 1983.

58. DOUGHERTY, N.S. Jr; STEINLE, F.W. Jr. — Transition Reynolds number comparison in several major transonic tunnels. AIAA Paper 74-627 1974.

59. DOUGHERTY, N.S. Jr; FISHER, D.F. — Boundary-layer transition on a slender cone in wind tunnels and flight for indications of flow quality. AEDC-TR-81-26 (AD-A111328), 1982.

60. BUCKNER, J.K.; WEBB, J.B. — Selected results from the YF-16 wind-tunnel test program. AIAA 76-619, 1974.

61. GREEN, J.E. — On the influence of free stream turbulence on a turbulent boundary layer, as it relates to wind tunnel testing at subsonic speeds. AGARD-R-602, Paper 2, 1974.

62. MIGNOSI, A.; ARNAL, D.; PRUDHOMME, S. — Problems connected with laminar flows in a cryogenic wind tunnel. DFVLR-Bericht 92-06, Paper 92-01-015, March 1992.

63. DOUGHERTY, N.S. Jr; FISHER, D.F. — Boundary layer transition on a 10 deg cone: wind tunnel/flight data correlation. AIAA 80-0154, January 1980.

64. ROBINSON, C.E.; BAUER, R.C.; NICHOLS, R.H. — Estimating water vapour condensation effects for transonic and supersonic flow fields. AIAA Paper 85-5020, 1985.

65. PHILPOTT, D.R. — A note on the effect of humidity on the properties of air and on wind tunnel testing. Memorandum 143, ESDU International, May 2005.

66. REASER, J.S.; HALLISY, J.B.; CAMPBELL, R.L. — Design and true Reynolds number 2-D testing of an advanced technology aerofoil. AIAA-83-1792, July 1983.

67. NIKURADSE, J. — Strömungsgesetzen rauhen Rohren. Forsch. Arb. Ing. Wes., 161, 1933.

68. EARNSHAW, P.B.; GREEN, A.R.; HARDY, B.C.; JELLY, A.R. — A study of the use of half-models in high-lift wind tunnel testing. AGARD-CP-515, Paper 20, September 1993.

69. PHILPOTT, D.R. — The use of VGK in an approximate method to determine the minimum surface roughness height which influences turbulent boundary layer skin friction. Memorandum 144, ESDU International, May 2005.

KEEPING UP TO DATE

Whenever Items are revised, subscribers to the service automatically receive the material required to update the appropriate Volumes. If you are in any doubt as to whether or not your ESDU holding is up to date, please contact us.

Please address all technical engineering enquiries and suggestions to:

ESDU International plc	Tel:	020 7490 5151 (from the UK)
		+44 20 7490 5151 (from outside the UK)
	Fax:	020 7490 2701 (from the UK)
		+44 20 7490 2701 (from outside the UK)
	E-Mail:	esdu@esdu.com
	Website:	www.esdu.com

For users in the USA, please address all Customer Service and Support enquiries and suggestions to:

IHS Engineering Products	Tel:	1 800 447 3352 (toll free number)
and	Fax:	1 303 397 2599
Global Engineering Documents	Website:	www.ihs.com www.global.ihs.com

ESDU 05022

Extrapolating wind-tunnel data to full-scale reynolds number. Part 1: Principles
ESDU 05022

ISBN 1 86246 574 6, ISSN 0141-4356

Available as part of the ESDU Series on Transonics. For information on all ESDU validated engineering data contact ESDU International plc, 27 Corsham Street, London N1 6UA.

ESDU 05022 gives an introduction to the principles of dynamic similarity and its application to wind-tunnel testing, with particular reference to the testing of transport configurations in the transonic speed range. Inherent limitations that prevent the complete achievement of dynamic similarity in a wind-tunnel test are described.

Scale effects arising from the influence of Reynolds number on the boundary layer are discussed and particular reference is made to transition, separation and shock wave-boundary layer interaction. Phenomena associated with wind-tunnel testing but which may be interpreted, erroneously, as a genuine Reynolds number dependency in the flow under examination (pseudo Reynolds-number effects) are also discussed.